HF Radar Performance in a Low-Energy Environment: CODAR SeaSonde Experience on the West Florida Shelf*

YONGGANG LIU, ROBERT H. WEISBERG, AND CLIFFORD R. MERZ

College of Marine Science, University of South Florida, St. Petersburg, Florida

SAGE LICHTENWALNER

Institute of Marine and Coastal Sciences, Rutgers, The State University of New Jersey, New Brunswick, New Jersey

GARY J. KIRKPATRICK

Mote Marine Laboratory, Sarasota, Florida

(Manuscript received 26 June 2009, in final form 2 April 2010)

ABSTRACT

Three long-range (5 MHz) Coastal Ocean Dynamics Application Radar (CODAR) SeaSonde HF radars overlooking an array of as many as eight moored acoustic Doppler current profilers (ADCPs) have operated on the West Florida Shelf since September 2003 for the purpose of observing the coastal ocean currents. HF radar performance on this low-energy (currents and waves) continental shelf is evaluated with respect to data returns, the rms differences between the HF radar and the ADCP radial currents, bearing offsets, and radial velocity uncertainties. Possible environmental factors affecting the HF radar performance are discussed, with the findings that both the low-energy sea state and the unfavorable surface wave directions are the main limiting factors for these HF radar observations of currents on the WFS. Despite the challenge of achieving continuous backscatter from this low-energy environment, when acquired the data quality is good in comparison with the ADCP measurements. The rms differences range from 6 to 10 cm s^{-1} for hourly and from 3 to 6 cm s^{-1} for 36-h low-pass-filtered radial currents, respectively. Bearing offsets are in the range from −15° to +9°. Coherent variations of the HF radar and ADCP radial currents are seen across both tidal and subtidal frequency bands. By examining the HF radar radial velocities at low wave energy, it is found that the data returns decrease rapidly for significant wave heights smaller than 1 m, and that the rms differences between the HF radar and ADCP radials are degraded when the significant wave height is smaller than 0.3 m.

1. Introduction

Descriptions of the West Florida Continental Shelf (WFS) circulation have evolved along with coastal ocean circulation-observing technologies. Early inferences on surface currents were limited to drift bottles (e.g., Tolbert and Salsman 1964). More advanced satellite-tracked drifters were applied later (e.g., Ohlmann and Niiler 2005), but because of the Lagrangian nature of drifters some areas were inadequately sampled, for example, the "forbidden zone" on the southeastern part of the WFS described by Yang et al. (1999). Measurements with in situ moorings began in the 1970s (e.g., Niiler 1976; Price et al. 1978; Weatherly and Martin 1978; Blaha and Sturges 1981; Mitchum and Sturges 1982; Marmorino 1983a,b; Halper and Schroeder 1990; Weatherly and Thistle 1997); however, with conventional single-point current meters, velocities were measured at only a limited number of water column depths. Measurements with acoustic Doppler current profilers (ADCPs) began in 1993, first at a single location—midshelf on the 47-m isobath—and then at multiple locations across the shelf (e.g., Weisberg et al. 1996, 2000, 2001, 2005, 2009; Meyers et al. 2001; Liu and Weisberg 2005a,b, 2007). These ADCPs measured currents across most of the water column from the near surface to near bottom, but still with limited horizontal coverage.

* Center for Prediction of Redtide Contribution Number 7.

Corresponding author address: Yonggang Liu, College of Marine Science, University of South Florida, 140 Seventh Ave. South, St. Petersburg, FL 33701.
E-mail: yliu18@gmail.com

DOI: 10.1175/2010JTECHO720.1

High-frequency (HF) radars are designed to sample surface currents over large horizontal extents and at high spatial resolution. Applications are now found over much of the world's coastal oceans. Examples abound on the U.S. Pacific coast (e.g., Barrick et al. 1977; Paduan and Cook 1997; Lipphardt et al. 2000; Nishimoto and Washburn 2002; Beckenbach and Washburn 2004; Kosro 2005; Roughan et al. 2005; Kaplan et al. 2009; Kim et al. 2009), the U.S. Atlantic coast (e.g., Shay et al. 2002, 2008; Graber et al. 1996; Marmorino et al. 1999; Haus et al. 2000; Chant et al. 2004; Kohut et al. 2008; Roarty et al. 2008; Dzwonkowski et al. 2009; Parks et al. 2009), the European coastal seas (e.g., Prandle and Ryder 1985; Gurgel et al. 1999; Kovacevic et al. 2004; Cosoli et al. 2005; Abascal et al. 2009; Gacic et al. 2009; Molcard et al. 2009; Sentchev et al. 2009), and the Asian marginal seas (e.g., Takeoka et al. 1995; Yang et al. 2005; Ebuchi et al. 2006; Yoshikawa et al. 2007; Ichikawa et al. 2008; Zhu et al. 2008; Hisaki and Imadu 2009; Takahashi et al. 2009). In combination, HF radars and ADCPs provide a powerful system for observing the three-dimensional (3D) coastal ocean circulation (e.g., Paduan and Rosenfeld 1996; Shay et al. 1998; Shen and Evans 2001; Chant et al. 2004; Ullman and Codiga 2004; Liu et al. 2007). Such applications for the WFS are described by Kelly et al. (2002), using the Coastal Ocean Dynamics Applications Radar (CODAR) for 11 days in January 2001, and by Shay et al. (2007), using a Wellen Radar (WERA; Gurgel et al. 1999) operated in tandem with ADCPs for a 1-month proof-of-concept test in 2003.

Immediately following the short-term WERA experiment, a set of CODAR SeaSonde, long-range HF radars were deployed on the WFS in September 2003. These HF radars operate at a nominal frequency of 5 MHz, with the intended purpose of observing surface currents out to about 200 km offshore, thereby capturing both the inner shelf region, forced primarily by local winds and heat flux, and the outer shelf region, impacted by the Gulf of Mexico Loop Current. Such long-range, 5-MHz radars have a history of successful use elsewhere, such as the New Jersey shelf (Kohut et al. 2006; Ullman et al. 2006) and south of Sagami Bay, Japan (Ramp et al. 2008). Unlike these other locations the ocean surface wave climate on the WFS tends to be less energetic.

The importance of waves is due to the way that HF radars sense ocean surface currents. HF radar systems derive estimates of the surface velocity field from the surface gravity wave field via Bragg scattering of the HF radar transmitted beam, which returns to the receiver Doppler shifted by the Bragg wave interacting with the surface current (Crombie 1955; Lipa and Barrick 1983; Paduan and Rosenfeld 1996). Paduan and Rosenfeld (1996) and Lipa et al. (2006) discuss how combined current speed and wave amplitude affect performance. However, except for the short duration and shorter-range studies of Kelly et al. (2002) with a 25-MHz CODAR and Shay et al. (2007) with a 16-MHz WERA, low-energy (currents and waves) environments, such as the WFS, neither have been evaluated for HF radar performance nor have systematic evaluations of 5-MHz HF radar performance for surface current mapping using multiyear in situ current observations from moorings at multiple locations. Given such multiyear (2003–08) datasets, it is appropriate to review the CODAR SeaSonde experience on the WFS to both assess performance and explore the lower limit below which surface waves fail to facilitate long-range current mapping on the WFS.

The paper is arranged as follows. In situ observations are described in section 2. Statistical metrics are given in section 3. HF radar performance is evaluated in section 4, where (i) the data returns are examined relative to the environmental factors, (ii) the HF radar accuracy is quantitatively assessed by comparing the radial velocity component estimates with measurements by moored ADCP, (iii) the direction-finding capability is evaluated, and (iv) the distribution of radial velocity uncertainty is shown for each radar site. Section 5 discusses the challenges of long-range HF radar observations on the low-energy WFS, and section 6 summarizes the findings.

2. Ocean current observations on the West Florida Shelf

a. CODAR array

Three long-range, CODAR SeaSonde HF radars operating at a nominal frequency of 5 MHz are presently deployed along the West Florida coast (Fig. 1). From north to south, the Redington Shores (27°49.937′N, 82°50.032′W), Venice (27°04.655′N, 82°27.096′W), and Naples (26°09.729′N, 81°48.632′W) sites started data collection on 24 September 2003, 27 April 2004, and 20 April 2005, respectively. Such 5-MHz radars estimate radial current velocity (radials) at an effective depth of ~2 m (Stewart and Joy 1974; Paduan and Graber 1997; Ramp et al. 2008), with nominal range and bearing resolutions of 5.8 km and 5°, respectively. Radials are processed using the CODAR SeaSonde software suite after directional calibration using measured antenna patterns as in Kohut and Glenn (2003). A community toolbox "HFR_Progs" (https://cencalarchive.org/~cocmpmb/COCMP-ki/index.php/Documentation:HFR_Progs) is used to remove the outliers and to interpolate the radial data onto uniform radial grids. The outliers, defined as radials with either unusually large speeds (>50 cm s^{-1}; the radial speed cutoff value in the processing software

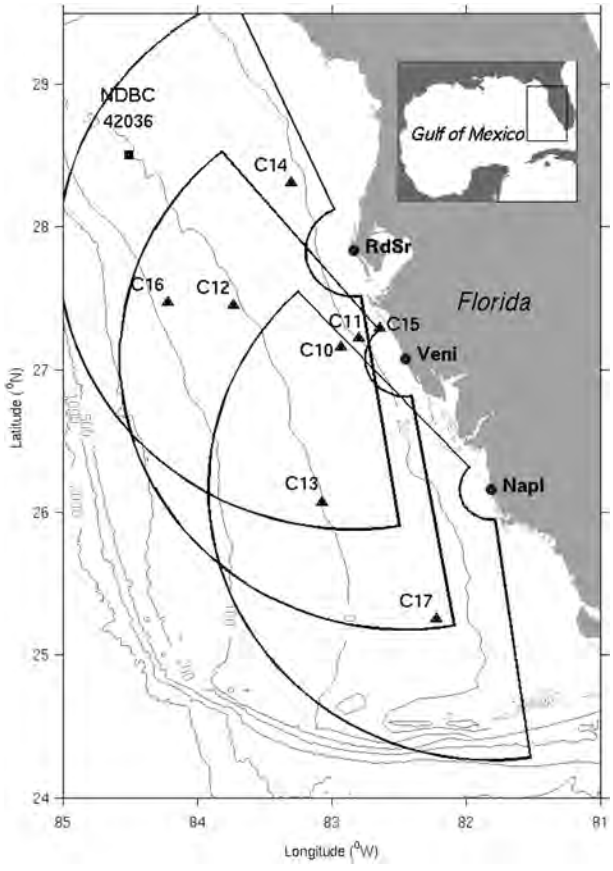

FIG. 1. Map of CODAR, ADCP mooring, and wave gauge deployments on the WFS. The areas enclosed by the arcs represent the HF radar radial spatial coverage for the three sites along the WFS: Redington Shores (RdSr), Venice (Veni), and Naples (Napl), respectively. Locations of the ADCP moorings (C11–C17) are indicated (solid triangles), and the wave gauges are located at moorings C11 and C15 and NDBC buoy 42036, respectively. Bathymetric contours show depths of 20, 50, 100, 200, 500, 1000, and 2000 m. A map of Gulf of Mexico is inserted in the upper-right corner.

was set to be 150 cm s^{-1}) or large temporal uncertainty (>10 cm s^{-1}), are removed prior to the interpolation. Other CODAR SeaSonde software suite–processing techniques are used to remove ionospheric contamination and very short bursts of interference/lightning, which would otherwise bias the FFT analysis for Doppler shift. Data gaps are filled by interpolation over one missing bin in range and two missing bins in bearing.

b. Moored ADCP array

Collocated on the WFS is a moored array of ADCPs. Initiated in 1993 with a single mooring at midshelf (e.g., Weisberg et al. 1996) the array evolved to the configuration used herein by 2003 (e.g., Weisberg et al. 2005; Liu and Weisberg 2005a). Figure 1 shows the moorings within the CODAR radial coverage domain corresponding to the observing period selected for analysis (September 2003–May 2008). The moored array include both bottom-mounted, upward-looking ADCPs (C11 and C15) and surface-mounted, downward-looking ADCPs (C12, C13, C14, C16, and C17), all measuring vertical profiles of current velocity throughout most of the water column. Among the seven moorings located from the 20- to 75-m isobaths, the depths of ADCPs' uppermost bins range from 3 to 5 m. Note that mooring C15 is not used for velocity comparison because it is located outside of the CODAR coverage area. Upon both quality control and editing, the ADCP velocity time series are archived hourly (e.g., Liu and Weisberg 2005a,b; Mayer et al. 2007), and Mayer et al. (2007) report no appreciable differences between upward- and downward-looking ADCPs that would impact this study. Time lines of moored ADCP data are shown in Fig. 2.

c. Other data

Other in situ observations include ocean wave and surface meteorological data. Wave gauges deployed at moorings C15 and C11 measured wave height, period, and direction at 4-h intervals at the 10- and 20-m isobaths, respectively, and the National Data Buoy Center (NDBC) buoy 42036 returned hourly wave data (online at http://www.ndbc.noaa.gov/station_page.php?station=42036) at the 55-m isobath (Fig. 1). Hourly wind data were obtained from the NDBC buoy 42036 and the NDBC Coastal-Marine Automated Network (C-MAN) station VENF1 at Venice, Florida (online at http://www.ndbc.noaa.gov/). The anemometer heights for the buoy and the C-MAN station are at 4 and 11.6 m above mean sea level, respectively. The winds were adjusted to a standard 10-m level prior to further analysis. Ocean wave hindcast reanalysis products of the third-generation Wavewatch III (Tolman 1991) version 2.22 regional western North Atlantic model were downloaded from http://polar.ncep.noaa.gov/waves/index2.shtml. Applications of Wavewatch III over many different ocean regions are discussed by Chu et al. 2004; Chu and Cheng 2008).

3. Statistical metrics

A widely used statistical measure of the agreement between two scalar time series is the correlation coefficient (CC) or its squared value, the coefficient of determination (r^2). These describe the covariability (in a linear least squares error sense) between the two time series, and they are used in conjunction with a linear regression coefficient (b) that scales the two time series. The mean square error (MSE) is also a commonly used measure of accuracy (e.g., Oke et al. 2002; Chu et al. 2004)

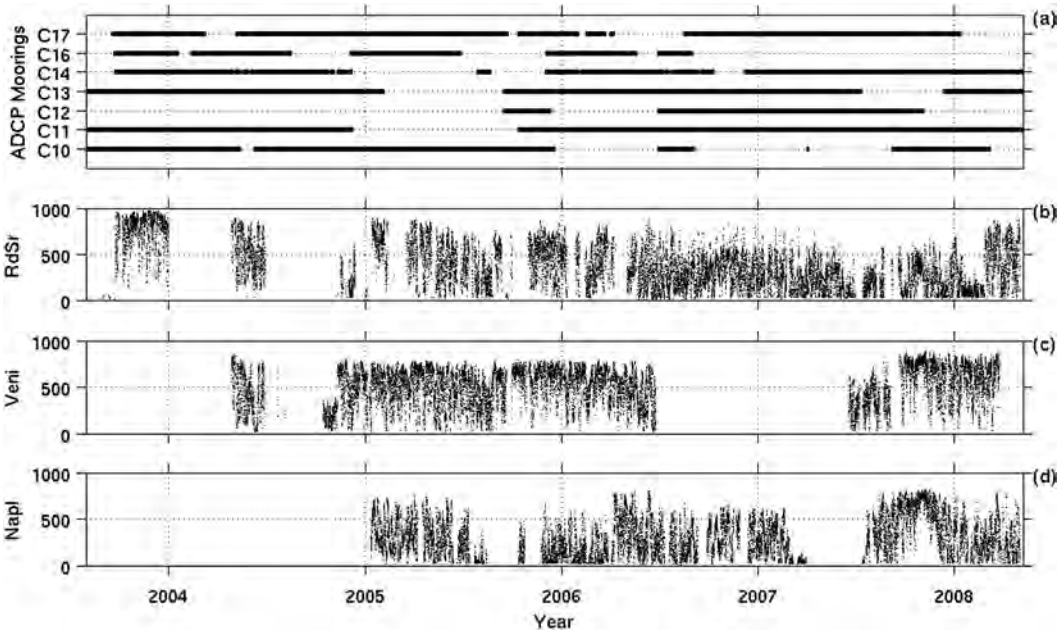

FIG. 2. (top) Time lines of moored velocity data availability and (bottom) time series of coverage, defined as the number of sectors returning data each hour, for the three HF radars: Redington Shores (RdSr), Venice (Veni), and Naples (Napl).

$$\mathrm{MSE} = \langle (V_{\mathrm{HF}} - V_{\mathrm{ADCP}})^2 \rangle, \tag{1}$$

where V_{HF} and V_{ADCP} are time series of radial currents measured by HF radar and ADCP, respectively, and $\langle\ \rangle$ denotes a mean. The MSE may be decomposed into three parts,

$$\mathrm{MSE} = \mathrm{MB}^2 + \mathrm{SDE}^2 + \mathrm{CCE}^2, \tag{2}$$

where $\mathrm{MB} = \langle V_{\mathrm{HF}} \rangle - \langle V_{\mathrm{ADCP}} \rangle$ is the mean bias error, $\mathrm{SDE} = S_{\mathrm{HF}} - S_{\mathrm{ADCP}}$, is the standard deviation error, and $\mathrm{CCE} = [2S_{\mathrm{HF}}S_{\mathrm{ADCP}}(1 - \mathrm{CC})]^{1/2}$, the cross-correlation error, and where $\langle V_{\mathrm{HF}} \rangle$ and $\langle V_{\mathrm{ADCP}} \rangle$ are the respective means and S_{HF} and S_{ADCP} are the respective standard deviations. In practice, rms difference (rmsd) is often used instead of MSE because rms has the same units as the variable. Based on the MSE, a skill score is presented by Willmott (1981), which, when applied to the HF radar and ADCP currents, is

$$\mathrm{WS} = 1 - \mathrm{MSE}/\langle (|V_{\mathrm{HF}} - \langle V_{\mathrm{ADCP}} \rangle| + |V_{\mathrm{ADCP}} - \langle V_{\mathrm{ADCP}} \rangle|)^2 \rangle. \tag{3}$$

Here, WS = 1 indicates perfect agreement, whereas WS = 0 indicates no agreement. Recently, WS was used to evaluate the performance of numerical ocean models (e.g., Warner et al. 2005; Wilkin 2006; Liu et al. 2009).

4. Performance evaluation of CODAR SeaSonde

a. Radial current data returns

1) TEMPORAL VARIATION

One indicator of HF radar performance is the spatial coverage of radials achieved over time. Following Shay et al. (1995) and Emery et al. (2004), coverage is defined as the number of sectors returning valid data each hour. Here the coverage is used to quantify the radial current data returns. Time series of the radial coverage show considerable temporal variation (Fig. 2), modulated at both high and low frequencies.

The high-frequency variation is illustrated for all three sites using an 18-day interval from 12 to 30 December 2008 (Fig. 3a). A diurnal variation in coverage is apparent at the Redington Shores and Naples sites, but is obscured at the Venice site, where the coverage is generally larger than for the other two sites. Such diurnal variation in coverage is observed elsewhere; for instance, the U.S. west coast (e.g., Paduan and Rosenfeld 1996; Emery et al. 2004). Local wind observations during this period do not exhibit a diurnal sea breeze (Fig. 3b), and the dominant tidal current variations are semidiurnal (Fig. 3c). Thus, the diurnal variation in coverage does not result from winds or tidal currents; rather, it is due to changes in background radio noise caused, for example, by the diurnal variations in the ionosphere (e.g., Davies 1990).

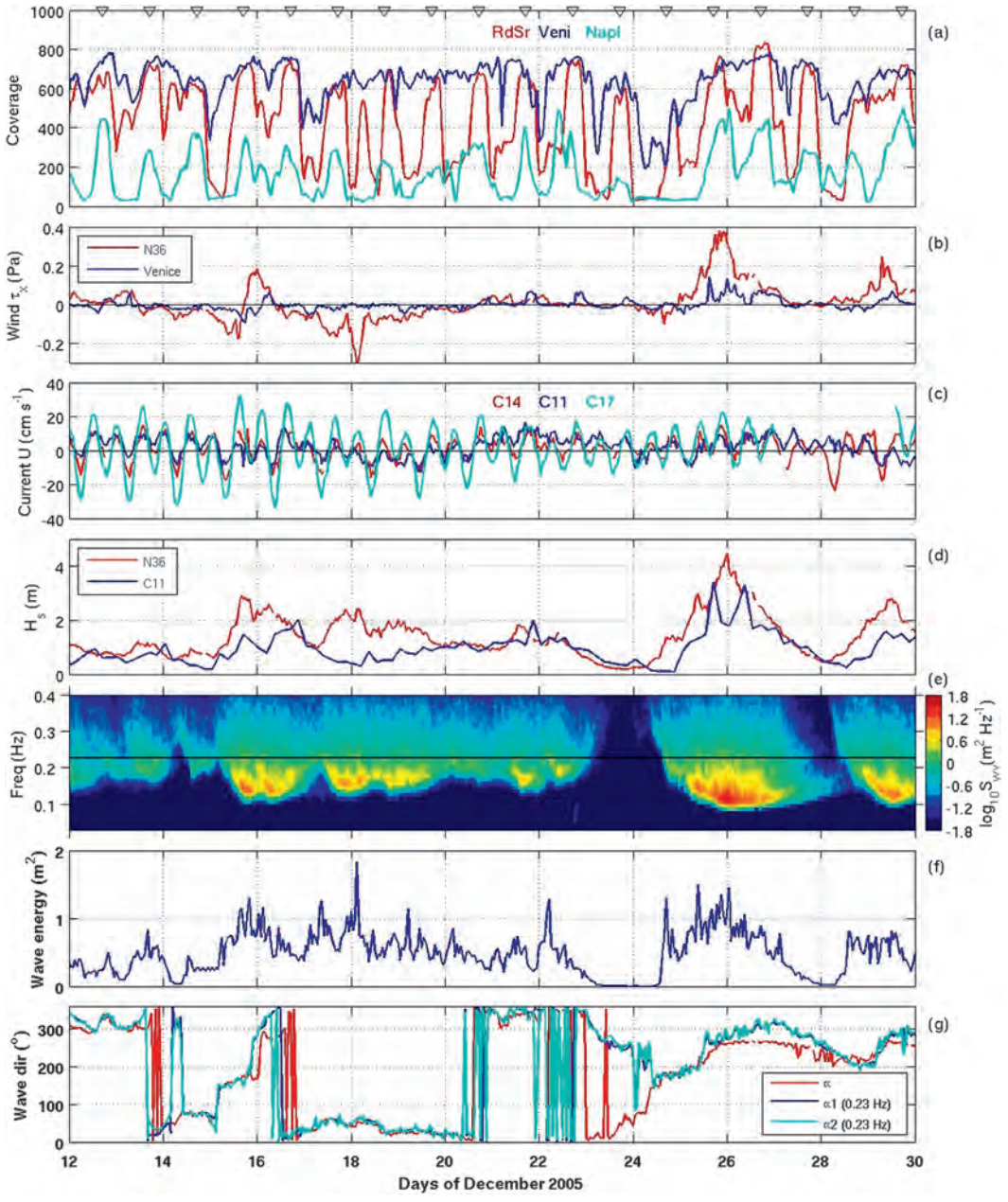

FIG. 3. Time series of (a) radial coverage from the three HF radar sites, Redington Shores (RdSr), Venice (Veni), and Naples (Napl), Florida; (b) wind east–west component at NDBC buoy 42036 and Venice; (c) surface current east–west component at moorings C14, C11, and C17; (d) significant wave height (H_s) observed at NDBC buoy 42036 and University of South Florida (USF) College of Marine Science mooring C11; (e) spectral wave energy at NDBC buoy 42036 (solid line indicates frequency of 0.23 Hz); (f) wave energy at frequency of 0.23 Hz; and (g) wave directions are measured from true north increase clockwise (0° = north, 90° = east): the direction from which the waves at the dominant period are coming (α), the mean (α_1), and the principal wave directions (α_2) at frequency of 0.23 Hz. The sampling intervals are 1 h for all the time series except the significant wave height at mooring C11, which was sampled every 4 h. The upside-down triangles on the top panel indicate local noon.

At lower frequencies (time scales of several days), the coverage variation correlates with the significant wave height H_s (Figs. 3a,d) and the spectral wave energy (Fig. 3e). Given that the sea state (H_s and wave energy) is modulated by winds, the radial data returns are similarly modulated on synoptic weather and longer time scales.

The Bragg scattering peak for a 5-MHz radar corresponds to a deep-water surface gravity wave of

approximately 0.23 Hz (a 4.4-s period). Based on the 36-h low-pass-filtered time series from November 2005 through March 2006 (5 months), the coefficients of determination r^2 between the coverage of the three radar sites from north to south and H_s at mooring C11 are 0.39, 0.34, and 0.30, respectively, and those with H_s at the NDBC buoy are 0.38, 0.30, and 0.18, respectively, all of which are significant at the 95% confidence level. The r^2 values between the coverage and the wave energy at 0.23 Hz measured at the NDBC buoy are 0.33, 0.32, and 0.07, respectively. Only the correlation for the Naples site ($r^2 = 0.07$) is not significant at 95% confidence, and this is likely due to the distance between the Naples site and the buoy rendering the wave energy quite different at these locations. Wave direction also matters. For example, whereas the wave energy at 0.23 Hz is generally lower during 12–14 than during 17–19 December 2005 (Fig. 3f), the radial coverage is generally higher (Fig. 3a). Note that the waves came from the northwest (300°–350°) during 12–14 December 2005, versus from those from the northeast (30°–60°) during 17–19 December 2005.

Monthly mean values of radial coverage, rms wind speed, H_s, and rms surface current speed are estimated from multiyear time series (Fig. 4), and these are used to examine the seasonal variation and relationship between different variables. For all three HF radar sites, monthly mean coverage values first decrease from April through July–August, and then increase from August to November, with minima in summer (Fig. 4a). These spring to fall changes are seen in the rms wind speed (Fig. 4b), rms current speed (Fig. 4c), H_s (Fig. 4d), and wave energy at a frequency of 0.23 Hz (Figs. 4e and 5). The monthly mean directional wave spectra climatology for the NDBC buoy 42036 from 1997 to 2008 (Fig. 5; see also, e.g., Steele et al. 1992; Earle et al. 1999) show that waves around 0.23 Hz come mainly from the north in winter (September–March) and from the south in summer (April–August). Waves from either the northeast (60°–90°) or the southwest (240°–270°) are mainly seen in winter months. Thus, the decreased radial coverage in summer appears to be related to both low sea state and smaller currents on the WFS in summer.

2) Spatial distribution

With the radial coverage varying on diurnal and longer time scales, Fig. 6 shows the spatial distribution of the percent of time for which radial coverage was achieved over the sampling duration (see the Fig. 2 time lines for each site). Percent coverage is calculated for each radial sector as the total number of estimates deemed valid divided by the total number of good radial mappings (each with 10 or more valid radial sectors at a time). Thus, the long gaps, for example, resulting from lightning damage, power outages, or computer-logging problems, are not taken into account in these percentages, because they do not affect the relative spatial distribution of the percentages. Among the three HF radar sites, Venice has the largest spatial coverage (with about 60% valid radial sectors extending offshore to about the 100-m isobath) and Naples has the smallest spatial coverage (with about 60% of the valid radial sectors limited to within the 50-m isobath).

Consistent among the three sites is a decrease in the percent temporal coverage with distance from the site origin (Fig. 6). For Redington Shores and Naples, most of the observed radial currents (with >70% coverage) are located within a small area (defined by about a 100-km range and a 60° bearing angle sector) mostly over the inner and midshelf regions; whereas for Venice these extend over a larger area (about 150 km in range and 120° in bearing angle), spanning the inner to the outer shelf.

The data returns are enhanced along some radial directions, and the angular distribution of the percent temporal coverage is not uniform across the field of view (Figs. 6a,b). This is due to distortions in the antenna response pattern caused by the near-field antenna environment (e.g., Barrick and Lipa 1986; Kohut and Glenn 2003; Emery et al. 2004; de Paolo and Terrill 2007; Cook et al. 2007; Laws et al. 2010). Both the measured and the ideal antenna patterns are superimposed on the coverage maps (where an angular smoothing of 10° was applied to the antenna patterns). The distortion of the measured from the ideal antenna patterns corresponds to the uneven distribution of the coverage across the bearing angles. Higher coverage is often seen over certain sectors with protruding (measured) antenna patterns (Figs. 6b,c). Additionally, when currents are weaker, there are fewer Doppler velocity determinations, making the radial spokes appear to be more evident.

A decrease in data returns with distance from the site antenna is expected, but why should the Venice site return more data than the other two sites? This may be due to the WFS wave climate, as is evident in the Wavewatch III model output, where the waves are larger over the central WFS than over the northern and southern WFS regions (see the Fig. 7 wave roses). That Naples exhibits the lowest data returns may be further exacerbated by its proximity to the Florida Keys to the south and the sheltering of waves propagating from the southeast (Fig. 7). Other factors that could result in different data returns among the sites include the transmitted power (cable attenuation), interference at the transmitted frequency, and the SNR of the Bragg-scattered returns.

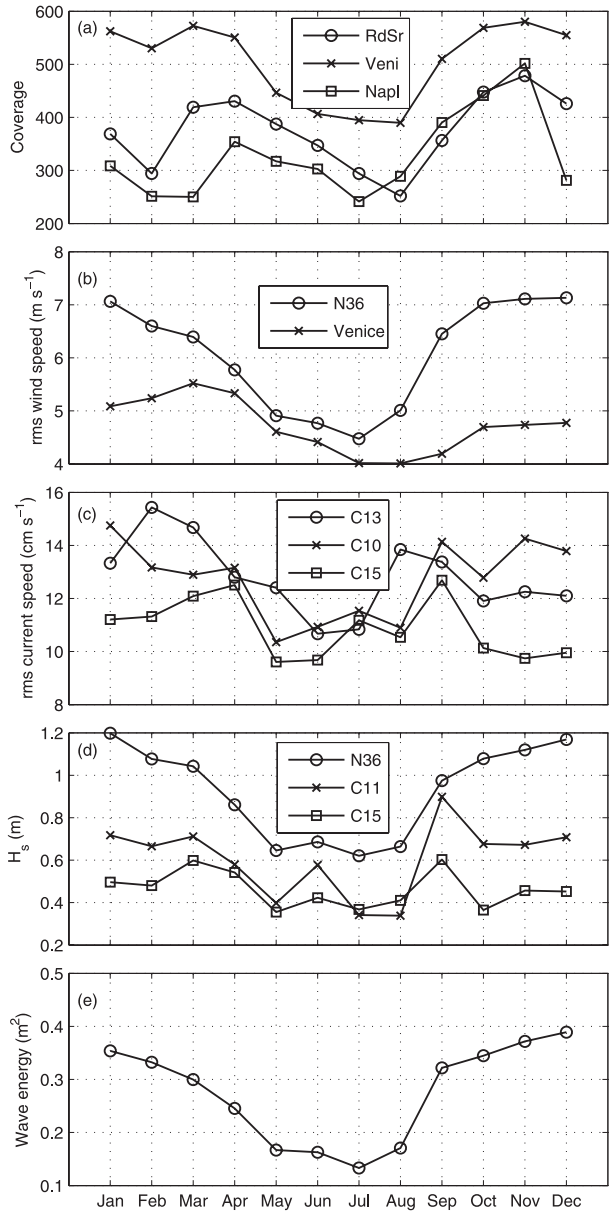

FIG. 4. Monthly mean climatology of (a) coverage of radial currents from the three HF radar sites: Redington Shores (RdSr), Venice (Veni), and Naples (Napl); (b) rms wind speed at NDBC buoy 42036 and Venice; (c) rms surface current speed at moorings C13, C10, and C15; (d) significant wave height (H_s) at the three moorings on the West Florida Shelf: NDBC buoy 42036, C11, and C15; and (e) wave energy measured at NDBC buoy 42036 at frequency of 0.23 Hz.

b. Comparison of HF radar and ADCP radial currents

Numerous evaluation studies exist in which HF radar surface current estimates are compared with other observations made with surface drifters, and ship-mounted and moored ADCPs (e.g., Shay et al. 1995; Paduan and Rosenfeld 1996; Chapman et al. 1997; Graber et al. 1997; Kosro et al. 1997; Kohut et al. 1999; Teague et al. 2001; Emery et al. 2004; Ullman and Codiga 2004; Ebuchi et al. 2006; Paduan et al. 2006). Some comparisons are based on radial currents (e.g., Kosro et al. 1997; Kohut et al. 1999; Emery et al. 2004; Paduan et al. 2006), while others use velocity vectors (e.g., Shay et al. 1995; Paduan and Rosenfeld 1996; Chapman et al. 1997; Graber et al. 1997; Teague et al. 2001; Ullman and Codiga 2004; Ebuchi et al. 2006). Here only radial current components are examined, the reasons for which are twofold. First, with velocity vectors requiring overlapping radial coverage from at least two sites, there is a much smaller subset of data for which vectors can be calculated relative to radials alone. Moreover, the accuracy of an HF radar-estimated vector is subject to the geometrical dilution of precision (GDOP; see, e.g., Chapman et al. 1997) owing to the angle at which the radials intersect. Second, and perhaps more important, is the fact that the radials themselves may be more useful for assimilation into coastal ocean circulation models than the vectors (e.g., Barth et al. 2008). Thus, given the utility of the radials along with their much larger availability, versus vectors, it makes sense to focus on the veracity of the radial velocity components.

1) TIME SERIES COMPARISONS

The radials from a CODAR site are bilinearly interpolated onto the mooring sites to get V_{HF}. The ADCP topmost bin velocities are rotated into a coordinate system aligned with the radial direction of the CODAR site to get V_{ADCP}. Hourly time series of these radial velocity components are shown in Fig. 8 for those sample durations when both HF radar and ADCP data are available and deemed valid. Comparison statistics between V_{HF} and V_{ADCP}, using the measures of section 3, are provided based on hourly and 36-h low-pass-filtered time series in Tables 1 and 2, respectively. For all 12 velocity pairs, the rmsd is in the range of 6–10 cm s^{-1} for hourly sampled radials and 3–6 cm s^{-1} for 36-h low-pass-filtered radials, respectively. Whereas the rmsd values for the hourly CODAR radials are larger than those of WERA ~(3.4–5.4) cm s^{-1} on the WFS (Shay et al. 2007), the multiyear records here are much longer than the approximate month-long records of Shay et al. (2007). Long time series include more extreme environmental conditions (stronger and weaker currents), so larger variability (rms) is expected. Additionally, more ADCP stations covering the inner to outer shelf regions are used here versus just the inner shelf in Shay et al. (2007). The MB values, within 2.5 cm s^{-1}, are comparable to those of Shay et al. (2007). A planned collocation of both CODAR and WERA on the WFS will clarify these in the near future.

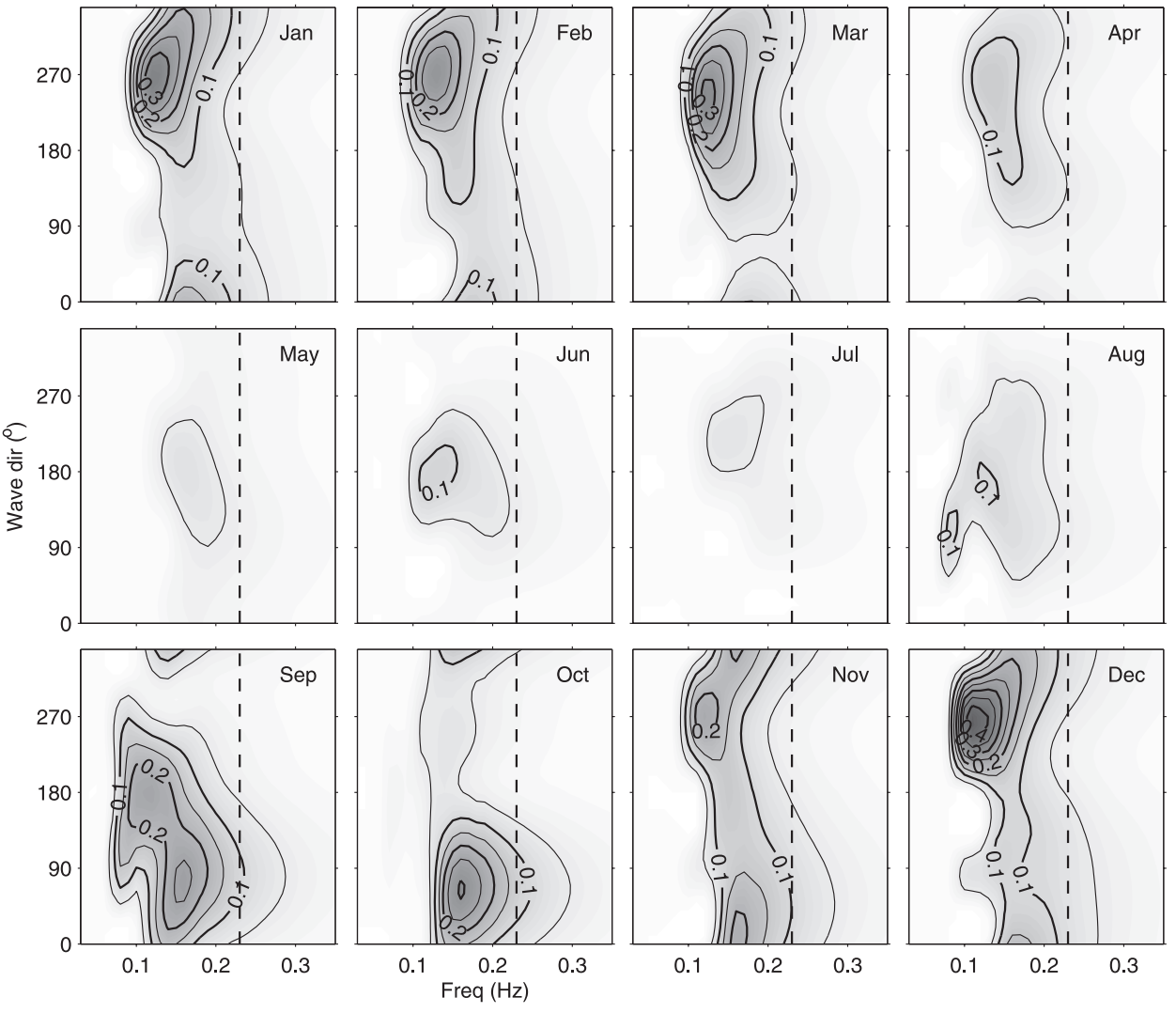

FIG. 5. Monthly mean climatology of directional wave spectrum (m^2 Hz^{-1}) measured at NDBC buoy 42036 during 1997–2008. The wave direction (the direction from which the waves are coming) measures from the true north and increases clockwise (0° = from north, 90° = from east). The dashed line corresponds to frequency of 0.23 Hz. The waves at 0.23 Hz mainly come from the north in winter (Sept–Mar), and from the south and southeast in summer (Apr–Aug).

Correlation determinants r^2 range between 0.35 and 0.68 for hourly and between 0.24 and 0.85 for low-pass-filtered time series, respectively, and the regression coefficients b, defined as $V_{ADCP} = b \times V_{HF} + c$, where c is a constant, are in the range of ~(0.65–0.95) for hourly and ~(0.46–1.04) for low-pass-filtered time series, respectively. The WS scores are ~(0.76–0.90) and ~(0.70–0.96), for hourly and low-pass-filtered time series, respectively.

Examples of the radial velocity pair V_{HF} and V_{ADCP} time series (both hourly and 36-h low-pass filtered) are shown for the three CODAR sites in Figs. 9–11, respectively. Coherent variations of V_{HF} and V_{ADCP} are seen on both tidal and subtidal time scales. With mooring C11 located on the edge of the Redington Shores radial coverage band, where data returns are low (Fig. 6), the radial velocity time series have more gaps there (Figs. 9c,d) than at the other mooring sites. For Venice, the most discontinuous time series is at mooring C16 (Figs. 10i,j), located at the outer edge of that radial coverage domain. Despite the location of mooring C17 relative to Naples (<40% data coverage), and the relatively weak currents there, the agreement between the V_{HF} and V_{ADCP} is surprisingly good, with rmsd, r^2, and b values of 7 cm s^{-1}, 0.55, and 0.89 for hourly time series, and 3 cm s^{-1}, 0.82, and 1.04 for 36-h low-pass-filtered time series, respectively (Figs. 11c,d).

Note that forming comparisons between currents measured with HF radar and with other instruments is intrinsically difficult for many reasons (e.g., de Paolo and Terrill 2007). First, these instruments sense different

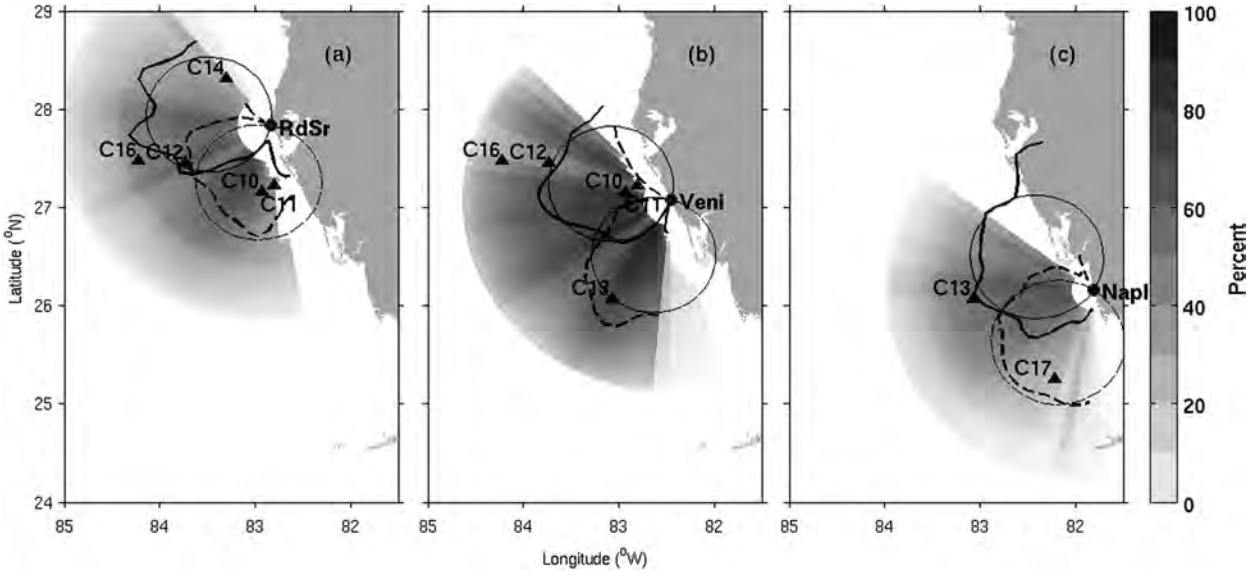

FIG. 6. Percent temporal coverage of valid radial currents for the three HF radar sites: (a) Redington Shores (RdSr), (b) Venice (Veni), and (c) Naples (Napl). Measured antenna patterns are superimposed [black bold lines; loops 1–3 (solid) and loops 2 and 3 (dashed)] and ideal antenna patterns are shown (thin dashed lines). The ADCP stations (solid triangles) for comparison are shown for each HF radar site.

quantities in their estimation of velocity; second, their sampling domain is also different, resulting in apparent errors by virtue of natural space–time environmental variability (Chapman et al. 1997; Kohut et al. 2006); and third, the sampling intervals differ. The HF radars output data as 3-hourly averages on an hourly basis, whereas the ADCPs (used here) record hourly data as averages of 360 one-second samples during the first 6 min of each hour (Liu and Weisberg 2007). Also, the instruments have inherent errors in angle and speed

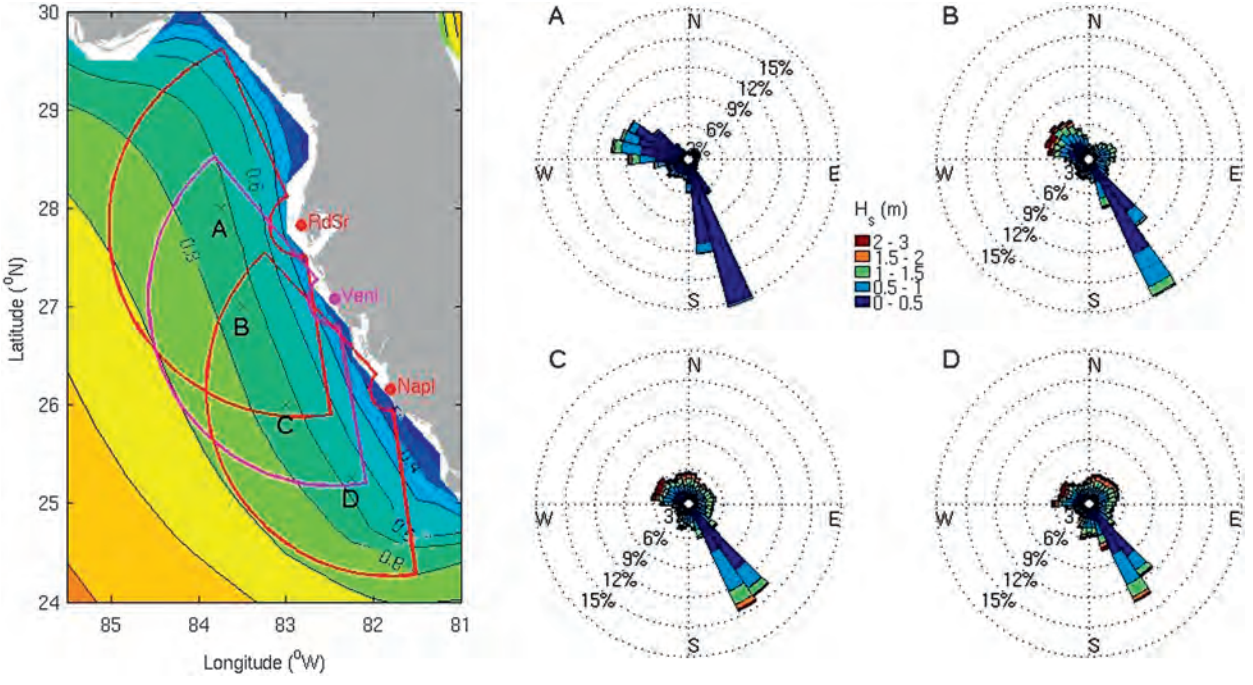

FIG. 7. (left) Map of mean significant wave height (H_s, m) superimposed with the HF radar radial spatial coverage. (right) Rose plots of peak wave direction (α) at selected locations (A, B, C, and D) on the West Florida Shelf from the Wavewatch III model output (1999–2007). The color scales indicate the corresponding H_s values. The circles designate the frequency of occurrence of the waves.

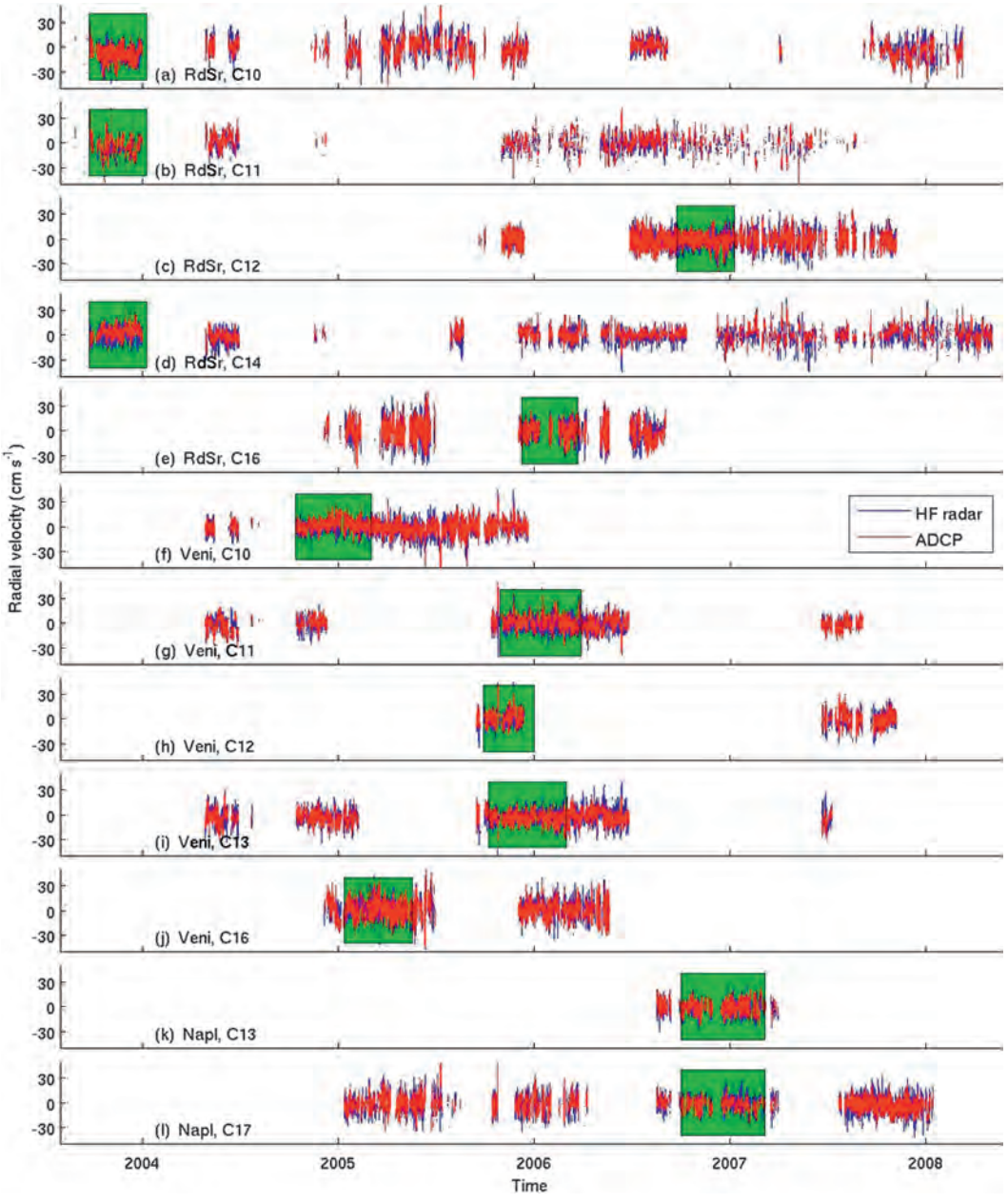

FIG. 8. Comparison of hourly HF radar and ADCP radial current time series at CODAR–ADCP velocity pairs during those periods when both CODAR and ADCP data are available: (a)–(e) velocity pairs for Redington Shores site, (f)–(j) velocity pairs for Venice site, and (k)–(l) velocity pairs for Naples site. The shaded periods will be zoomed-in in Figs. 9–11, respectively, for the Redington Shores, Venice, and Naples sites.

determination. In view of these intrinsic sampling differences the comparisons are deemed to be very good.

2) COMPARISON OF POWER SPECTRA

Gaps in the V_{HF} time series make it more difficult to compare the spectra of the CODAR and ADCP radials. Concurrent records of durations of about 3 months or longer in winter months (Figs. 8–11), however, do allow for the examination of variance on tidal and synoptic time scales. Prior to autospectral analysis small gaps were interpolated similar to the preprocessing in Emery et al. (2004).

The semidiurnal and diurnal tidal peaks are well resolved in the V_{HF} and V_{ADCP} spectra at all three sites (Fig. 12). Good agreement between surface (V_{HF}) and subsurface (V_{ADCP}) tidal variances is consistent with

TABLE 1. Comparison statistics of HF radar–ADCP hourly radial currents.

HF radar site	ADCP mooring	Start date	End date	Hours of data points	Rmsd (cm s^{-1})	MB (cm s^{-1})	r^2	b	c (cm s^{-1})	WS
RdSr	C10, 4 m	29 Aug 2003	9 Mar 2008	10 815	7	0.8	0.68	0.95	1	0.90
RdSr	C11, 4 m	29 Aug 2003	7 Sep 2007	5326	7	−2.3	0.65	0.76	−2	0.88
RdSr	C12, 4 m	20 Sep 2005	6 Nov 2007	8376	8	0.3	0.36	0.63	0	0.77
RdSr	C14, 4 m	23 Sep 2003	2 May 2008	12 301	8	−1.8	0.41	0.77	−1	0.78
RdSr	C16, 4 m	5 Dec 2004	1 Sep 2006	5197	10	−0.5	0.36	0.62	−1	0.77
Veni	C10, 4 m	27 Apr 2004	9 Mar 2008	13 743	6	−1.3	0.57	0.85	−1	0.86
Veni	C11, 4 m	27 Apr 2004	6 Sep 2007	9009	7	−0.8	0.43	0.65	−1	0.81
Veni	C12, 4 m	15 Sep 2005	6 Nov 2007	3482	8	−1.2	0.38	0.65	−1	0.78
Veni	C13, 5 m	27 Apr 2004	9 Jul 2007	9385	7	0.7	0.53	0.84	0	0.84
Veni	C16, 4 m	5 Dec 2004	20 May 2006	5900	10	1.5	0.35	0.56	2	0.76
Napl	C13, 4 m	17 Aug 2006	31 Mar 2007	2807	6	−1.2	0.47	0.77	0	0.81
Napl	C17, 4 m	11 Jan 2005	13 Jan 2008	9241	7	0.5	0.54	0.86	0	0.85

the barotropic nature of the semidiurnal and diurnal tidal currents (He and Weisberg 2002). At the lower-frequency synoptic time scales [a period of ~(2–16) days], agreement is also seen between the surface and subsurface radial variances, with the subsurface variances being slightly smaller, particularly at the 25-m isobath sites C10 and C17. These differences are consistent with wind-induced vertical shear (e.g., Richman et al. 1987; Emery et al. 2004; Kohut et al. 2006). At supertidal frequencies for all the three velocity pairs the V_{HF} are slightly higher than the V_{ADCP} variances, suggesting that the measurement error threshold is higher for the HF radar than for the ADCP.

3) COMPARISON OF TIDAL CONSTITUENTS

To further examine the CODAR capability for observing tidal currents, tidal analyses are performed on the same velocity pairs used in the autospectral analyses. The major tidal constituents (M_2, S_2, K_1, and O_1) are estimated using the T-TIDE toolbox (Pawlowicz et al. 2002), resulting in general agreements between the V_{HF} and the V_{ADCP} radial tidal constituents. For the Naples–C17, Redington Shores–C10, and Venice–C13 velocity pairs the differences between the V_{HF} and the V_{ADCP} radial tidal amplitudes for (M_2, S_2, K_1, and O_1) are (0.4, 0.5, −0.2, 0.1) cm s^{-1}, (−0.2, −0.5, −1.0, 0.5), and (1.0, 0.5, 0.0, 0.4), respectively. Similarly the V_{HF} and the V_{ADCP} radial tidal phase differences for (M_2, S_2, K_1, and O_1) are (−11, −13, 7, −10), (−19, −7, 1, −16), and (1, −2, 1, 9) degrees, respectively.

c. Bearing offset

Bearing offsets, the source for which is attributed to many factors, including the resolution capabilities of the combined receiving antenna and direction-finding algorithms (e.g., Barrick and Lipa 1986, 1997; Kosro et al. 1997; Laws et al. 2000; Emery et al. 2004; de Paolo and Terrill 2007), are present in nearly all direction-finding radars. The multiple signal classification (MUSIC) (Schmidt 1986) algorithm (with parameters: eigrat, sigprat, and diagrat set at 40, 20, and 2, respectively) may err in determining the direction of arrival of the incoming sea echo, thereby placing what may be correctly determined radial velocities into incorrect bearing sectors.

TABLE 2. Same as Table 1, but for 36-h low-pass-filtered time series.

HF radar site	ADCP mooring	Start date	End date	Hours of data points	Rmsd (cm s^{-1})	MB (cm s^{-1})	r^2	b	c (cm s^{-1})	WS
RdSr	C10, 4 m	29 Aug 2003	9 Mar 2008	7204	4	0.6	0.85	1.04	1	0.96
RdSr	C11, 4 m	29 Aug 2003	7 Sep 2007	1246	5	−1.9	0.77	0.68	−1	0.91
RdSr	C12, 4 m	20 Sep 2005	6 Nov 2007	4912	4	0.1	0.24	0.46	−1	0.70
RdSr	C14, 4 m	23 Sep 2003	2 May 2008	6840	4	−1.3	0.79	1.01	−1	0.93
RdSr	C16, 4 m	5 Dec 2004	1 Sep 2006	2999	6	−0.3	0.26	0.53	0	0.72
Veni	C10, 4 m	27 Apr 2004	9 Mar 2008	10 988	4	−1.3	0.77	0.92	−1	0.93
Veni	C11, 4 m	27 Apr 2004	6 Sep 2007	7145	4	−0.8	0.74	0.72	−1	0.92
Veni	C12, 4 m	15 Sep 2005	6 Nov 2007	2227	3	−0.9	0.65	0.82	−1	0.89
Veni	C13, 5 m	27 Apr 2004	9 Jul 2007	6918	4	0.7	0.66	0.79	0	0.90
Veni	C16, 4 m	5 Dec 2004	20 May 2006	3253	5	2.3	0.49	0.61	2	0.80
Napl	C13, 4 m	17 Aug 2006	31 Mar 2007	1370	3	−1.0	0.53	0.78	1	0.84
Napl	C17, 4 m	11 Jan 2005	13 Jan 2008	4590	3	0.7	0.79	0.98	−1	0.93

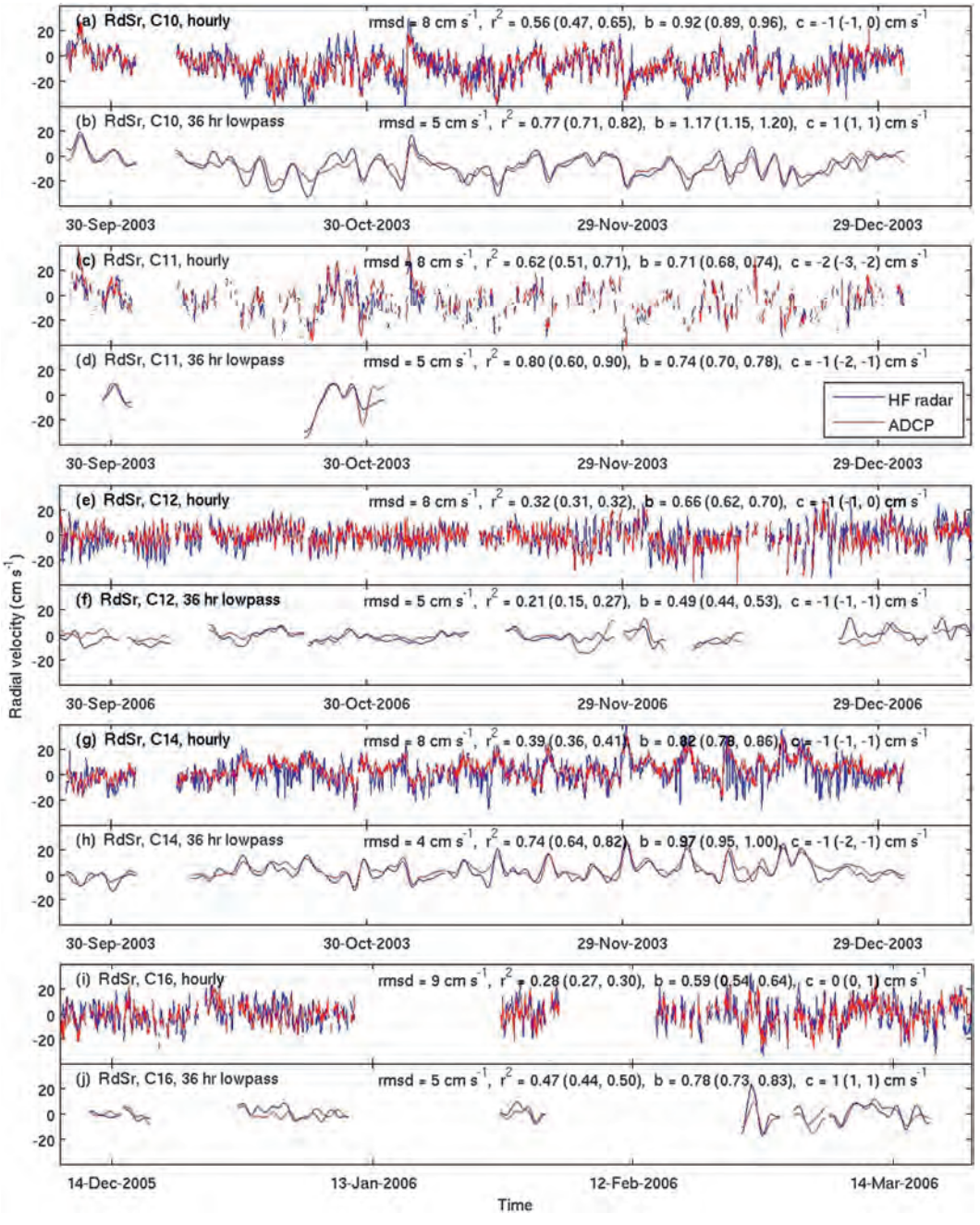

FIG. 9. Comparison of hourly and 36-h low-pass-filtered HF radar and ADCP radial current time series during selected periods for the Redington Shores (RdSr) site: moorings (a),(b) C10, (c),(d) C11, (e),(f) C12, (g),(h) C14, and (i),(j) C16. Statistics are shown on the upper-right corner of each panel: rms difference (rmsd), correlation of determination (r^2), regression coefficient (b), and intercept (c), with their 95% confidence levels in the parentheses, estimated following Emery and Thomson (2001, p. 253).

The direction-finding performance of the CODAR SeaSonde is investigated following Emery et al. (2004). For a given range to a radar site, corresponding to a given mooring location, all of the V_{HF} are sampled for all of the bearing angle sectors and then correlated with the V_{ADCP} at the given mooring location. Thus, with V_{ADCP} fixed and V_{HF} varying over all radial sector bins for a given radial range, the bearing angle sector exhibiting the highest correlation is thought to be the one that is most indicative of the correct radial value. With no offset the radial sector containing the mooring would be expected to exhibit the highest correlation, but this is not

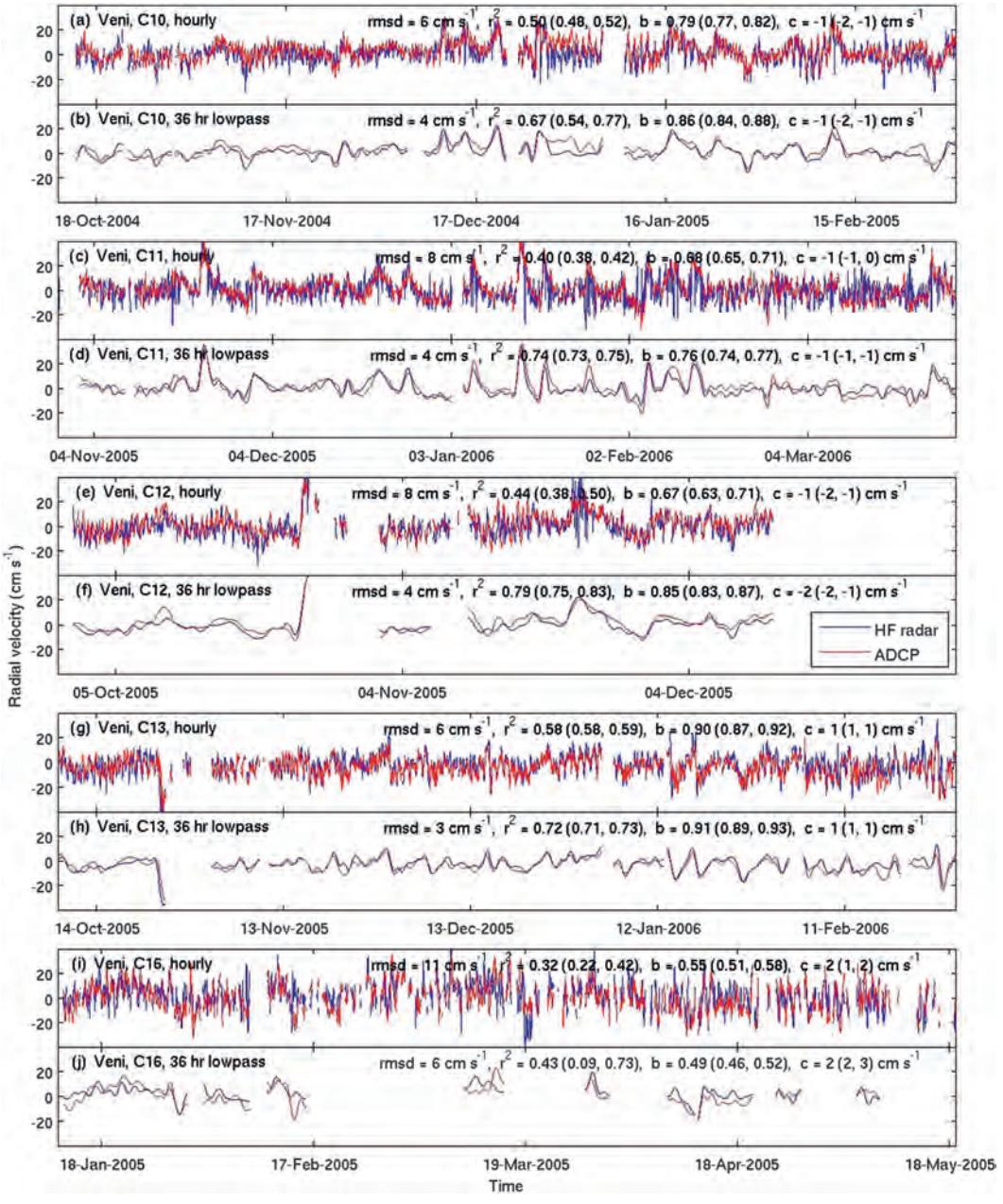

FIG. 10. As in Fig. 9, but for the Venice site and moorings (a),(b) C10, (c),(d) C11, (e),(f) C12, (g),(h) C13, and (i),(j) C16.

always the case. Bearing offset is therefore defined as $\Delta\theta = \theta_r - \theta_m$, where θ_m is the bearing to the mooring, and θ_r is the bearing to the center of the sector with the maximum V_{ADCP} and V_{HF} correlation (r^2), with positive $\Delta\theta$ indicating that the sector is displaced clockwise from the mooring.

Bearing offset analysis results are provided for all of the HF radar–ADCP pairs in Fig. 13. The r^2 values are shown for each pair as a function of bearing along with vertical lines indicating the bearing to the particular radar and the bearing corresponding to the maximum r^2, the offsets being defined as the differences between these two vertical lines. Among the 12 comparisons, 7 show that the peak r^2 is correctly positioned within the 5° sector where V_{ADCP} is measured, that is, $|\Delta\theta| \leq 5°$; and 3 show the peak r^2 displaced into a neighboring sector ($6° \leq |\Delta\theta| \leq 10°$). The Venice site exhibits the best direction-finding performance, with zero bearing offset at mooring C10 and only one case for which $|\Delta\theta| > 5°$ at mooring C11 (Fig. 13g), located on the 20-m isobath, and hence at short radar range (Fig. 1). The Naples site exhibits the largest bearing offset (−15°), as found for

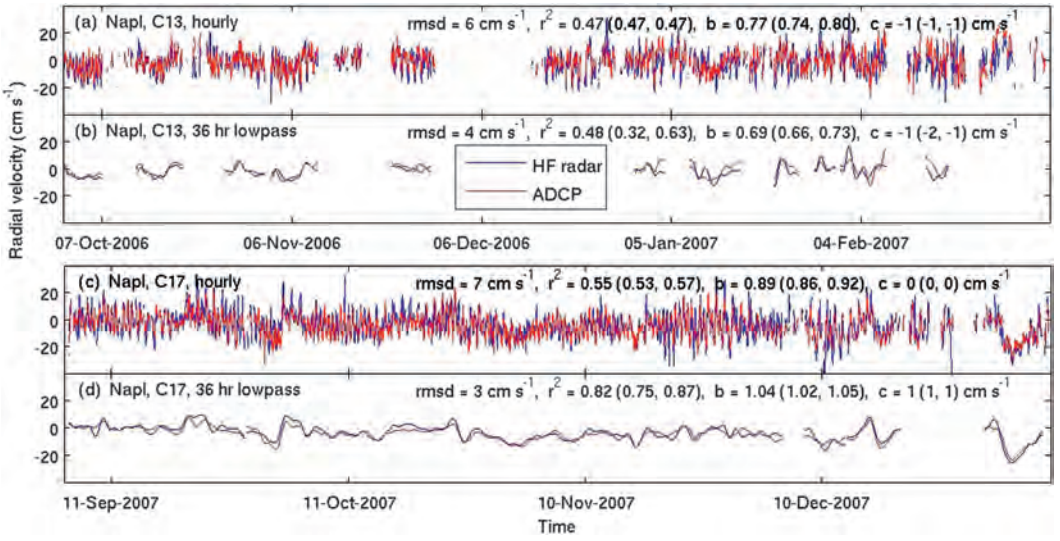

FIG. 11. As in Fig. 9, but for the Naples site and moorings (a),(b) C13 and (c),(d) C17.

mooring C17 (Fig. 13l), where the HF radar returns are relatively low (Fig. 6). The second largest bearing offset (−13°) is found at the Redington Shores site corresponding to mooring C11 (Fig. 13b). These bearing offsets found on the WFS are slightly smaller than those found for the 13-MHz CODAR SeaSonde on the U.S. west coast (Emery et al. 2004), although it is pointed out that differences in correlation used to assign bearing offsets are not significant at the 95% confidence level except for the Venice radar at mooring C11 (Fig. 13g).

d. Radial velocity uncertainties

The CODAR software provides spatial and temporal quality factors along with the radial velocity determinations. These quality factors, calculated as spatial and temporal standard deviations of the radials, indicate measurement uncertainty resulting from changing surface current patterns, horizontal shears over each radial sector, and systems noise levels. The CODAR manuals (Lipa 2003; Lipa et al. 2006) attribute most spatial uncertainty to horizontal current shear and most temporal uncertainty to time-varying current patterns. The quality factors are examined here with emphasis on their relationship to the rmsd between V_{HF} and V_{ADCP} and the antenna patterns.

In general, the mean radial velocity uncertainty is lower near the site origin and higher toward the outer bound of the radial coverage area (Fig. 14). These velocity uncertainty values are closely related with the rmsd between V_{HF} and V_{ADCP} in Table 1. Moorings in the large uncertainty area also have large rmsd values, and vice versa. For example, in Venice coverage area (Fig. 14b) the spatial uncertainties at moorings C16 and C12 (8.3 and 7.8 cm s^{-1}, respectively) are larger than those at moorings C10, C11, and C13 (5.0, 4.6, and 6.3 cm s^{-1}, respectively), and so are their rmsd values (10 and 8 cm s^{-1} versus 6, 7 and 7 cm s^{-1}, respectively). The uncertainty values are ~(1–2) cm s^{-1} smaller than the rmsd values at the Venice and Naples sites, but ~(3–4) cm s^{-1} smaller than the rmsd values at the Redington Shores site, indicating a lower bound on the actual uncertainty in the current velocity.

The spatial distribution of the mean radial uncertainty has an opposite trend with that of the data return (Fig. 6), that is, closer to the site origin the uncertainty is lower but the coverage is higher, and vice versa. Spoky features are also seen in some radial directions on the uncertainty maps (e.g., Fig. 14a). Like those on the coverage maps, they are mainly attributed to the distortion of the antenna patterns. The larger uncertainty values (>12 cm s^{-1}) in the southern portion of the WFS, mainly seen in the Naples site spatial coverage (Figs. 14c,f), are also seen in the southeastern corners of the Redington Shores and Venice sites' radial coverage (Figs. 14a,b). These findings may be related to low wave energy and unfavorable wave direction resulting from blocking by the Florida Keys.

5. Challenges of HF radar observation on the West Florida coast

The many data gaps in our multiyear HF radar archives (Fig. 2) are reflective of HF radar observational challenges on the WFS. Low data returns, especially in summer, are mainly due to the lower WFS summer energy environment and its corresponding lack of sufficient

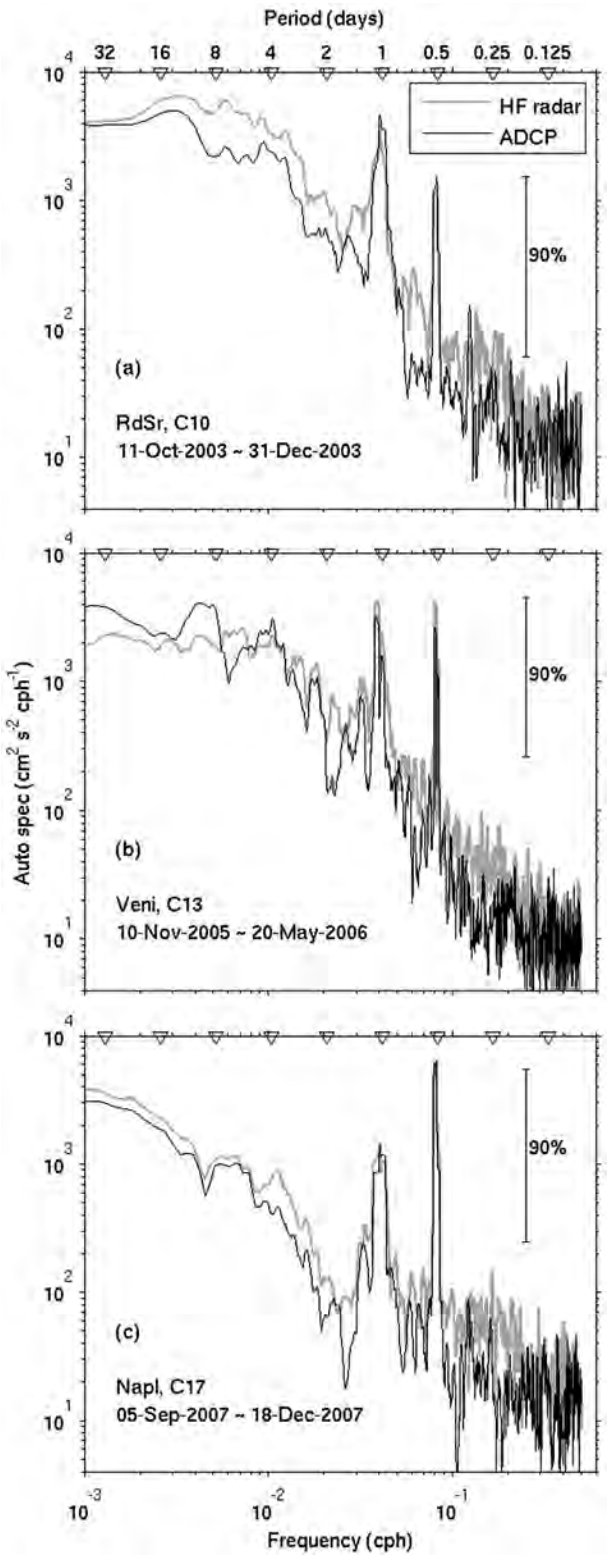

FIG. 12. Comparison of autospectra of HF radar and ADCP radial currents for three CODAR–ADCP velocity pairs: (a) RdSr–C10, (b) Veni–C13, and (c) Napl–C17. The starting and end dates of the analyzed time series are shown in each panel.

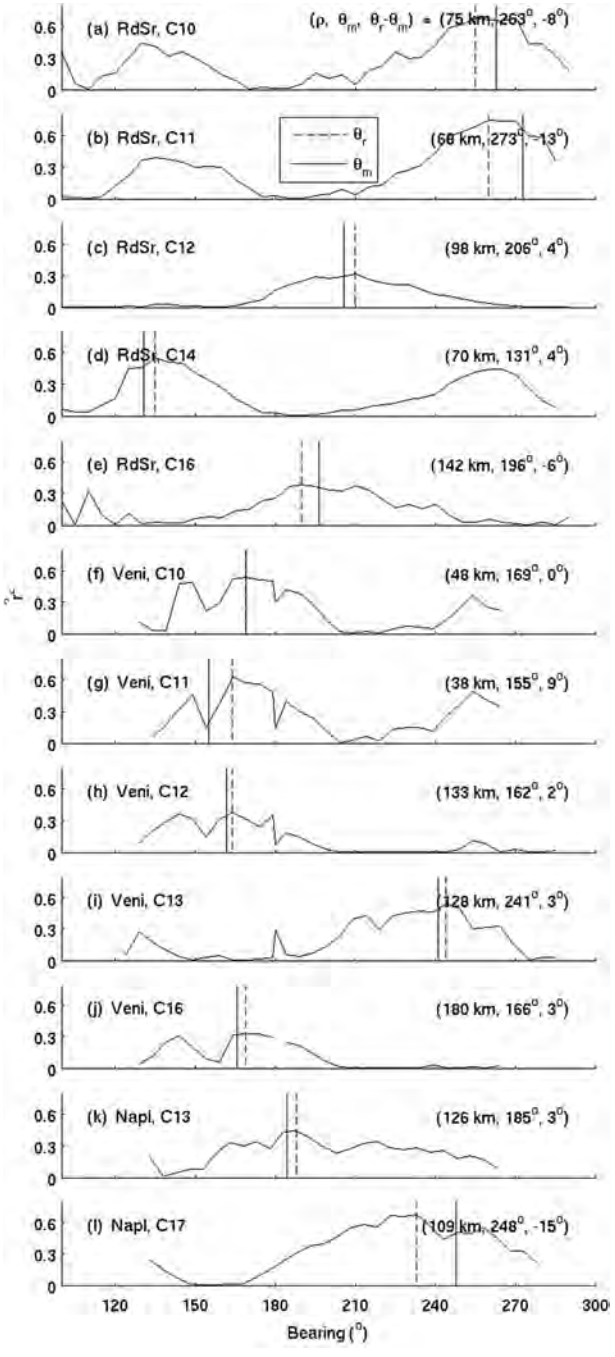

FIG. 13. Bearing offset (θ_r–θ_m) for all the HF radar and ADCP station pairs, where θ_r is the bearing to the center of the sector with maximum correlation (r^2) between the HF radar and ADCP radial currents, and θ_m is the bearing to the mooring. Solid lines indicate r^2 values along a certain ranges (ρ) of HF radar corresponding to the ADCPs locations.

wave energy in the band that is necessary for Bragg scattering at the selected transmit frequency. With summer monthly mean rms wind speed at NDBC buoy 42036 less than 5 m s^{-1} (Fig. 4b), the summer monthly

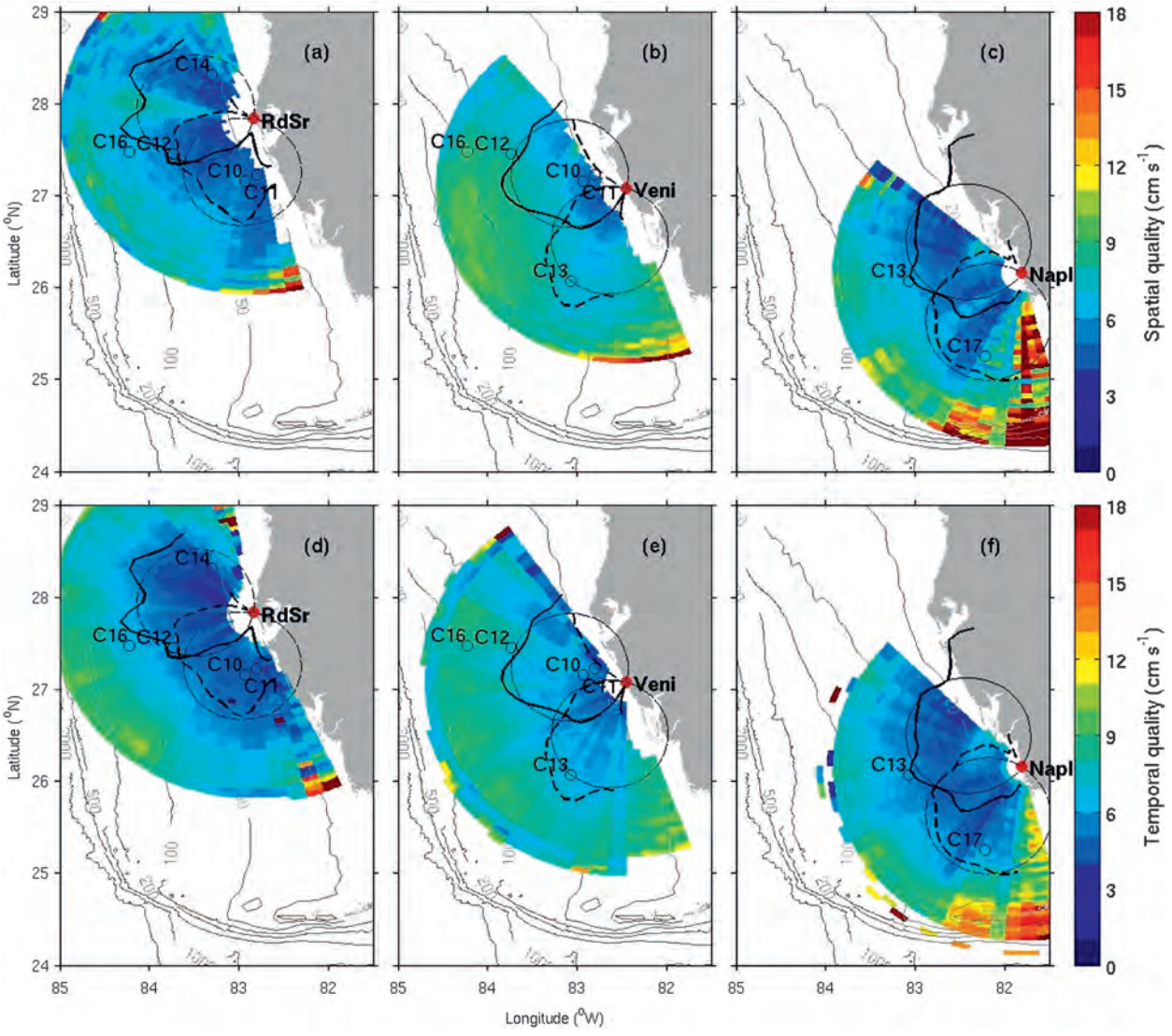

FIG. 14. Record-long mean (top) spatial and (bottom) temporal quality factors (or uncertainties) of the radial currents for each range-bearing cell of the three HF radar sites: (a),(d) Redington Shores (RdSr), (b),(e) Venice (Veni), and (c),(f) Naples (Napl). Measured antenna patterns are superimposed [black bold lines; loops 1–3 (solid) and loops 2 and 3 (dashed)], and ideal antenna patterns are shown (thin dashed lines). The ADCP stations (solid triangles) for comparison are shown for each HF radar site. The idealized antenna pattern was used prior to the measured beam pattern was available.

mean H_s there is less than 0.7, and even less (0.4 m) near the coast (Fig. 4c). Similarly, the WFS monthly mean rms surface current speed is generally less than 11 cm s^{-1} during summer months (Fig. 4d), and this agrees with analyses of WFS-moored ADCPs over a 3-yr interval of ~(1998–2001) (Liu and Weisberg 2005b; Liu et al. 2006), where greater than 90% of the subtidal current velocities were found to be weaker than 10 cm s^{-1}. This is in contrast with typical currents observed by HF radars in other coastal oceans, for example, currents on the U.S. west coast ~(10–30) cm s^{-1} (see, e.g., Kosro 2005; Kaplan et al. 2005; Kim et al. 2008) and currents affected by the strong western boundary currents, Kuroshio (Ramp et al. 2008) and Gulf Stream, and their mesoscale eddies (Shay et al. 1995).

Direction-finding systems suffer from the problem of low radial data coverage if the range of ocean current speed is small regardless of the signal-to-noise ratio [SNR; the ratio of the radar signal power to the noise power; see, e.g., Paduan and Rosenfeld (1996)]. The effect of low current speed is to make the Bragg peak spectrum narrower, thus resulting in less Doppler bins (radial velocity) for the direction-finding analysis. The less resolvable radial velocity values leads to poorer

coverage. The velocity resolution is dictated by the length of the time series used for the spectrum processing [i.e., the fast Fourier transform (FFT) length]; the longer the FFT length, the lower value of the minimum resolvable velocity, and vice versa. For our 5-MHz radar systems, the numerical resolution of the CODAR SeaSonde processing algorithms is 2.9 cm s^{-1} (with the default FFT length of 1024 points). An investigation was made into increasing velocity resolution to 1.5 cm s^{-1} by increasing the FFT length to 2048 points, but no significant improvement was found in coverage.

Additionally, HF radar current measurements rely on the existence of sufficiently large waves of a particular wavelength traveling with a component projecting onto a radial either toward or away from the radar. For the three HF radars on the west Florida coast, the most favorable wave directions would be across shelf, that is, propagating from the Gulf of Mexico to the Florida coast or away from the coast. However, the primary and peak wave directions on the WFS are mainly in the along-shelf direction (Figs. 5 and 7), which are not favorable for the HF radar current observations.

The mean H_s values at the NDBC buoy 42036 (based on 11 yr) and at moorings C11 and C15 (based on 2 yr) are 0.94, 0.63, and 0.47 m, respectively. The percentages of time for $H_s < 1$ m at these NDBC buoy 42036, C11, and C15 locations are 65%, 83%, and 92%, respectively. In summer, these percentages increase to 84%, 93%, and 96%, respectively, and the summer (May–August) mean H_s values decrease to 0.65, 0.42, and 0.39 m, respectively. Relatively low H_s values make the WFS a less favorable environment for HF radar than the U.S. east coast where the mean $H_s > 1$ m (Komar and Allan 2008) or the U.S. west coast where the mean $H_s > 2$ m (Menéndez et al. 2008). Unfavorable wave directions and low H_s on the WFS when combined with small current speeds, especially in summer months, yield relatively low data returns and/or rms radial current errors that at times may be similar to the currents being observed.

An instructive question is how low is too low for wave energy on the WFS to facilitate surface current mapping by HF radar. To address this, we estimated conditional averages of data coverage, rms wind speed, and data quality (indicated by the rmsd difference between V_{HF} and V_{ADCP}) all binned by the H_s and the wave energy at 0.23 Hz as measured at NDBC buoy 42036 (Fig. 15). With large waves (H_s approaching 2 m) the HF radar coverage reaches their mean peak values. This coverage decreases with decreasing wind and waves, and the coverage decreases rapidly once H_s becomes less than 1 m. Interestingly, while coverage decreases with H_s, the data quality (as measured by the rmsd between V_{HF} and V_{ADCP}) does not change appreciably until $H_s < 0.3$ m, corresponding to an rms wind speed of <3 m s^{-1} at the NDBC buoy location. Of course, when $H_s < 0.3$ m, the number of data points for averaging also decreases. Figure 15 also shows a similar relationship between the coverage and wave energy at 0.23 Hz. Whereas the rmsd between V_{HF} and V_{ADCP} gradually increases from 5 to 6 cm s^{-1} with the decreasing wave energy, both the decrease in coverage and the increase of the rmsd values become more pronounced when the spectral wave energy at 0.23 Hz is less than a threshold of 0.2 m^2.

As a consistency check, the SNR threshold is analyzed following a procedure in Fernandez et al. (2000). The SNR data are available from 24 July 2007 to 2 May 2008 (283 days) for the three sites. An average of the three channels (loops 1 and 2 and the monopole) is used to form a time series for each site. On average, among the three sites, about 85% of the time the SNR is above 10 dB, which is adequate for current mapping (Fernandez et al. 2000). This corresponds to an H_s value of 0.5 m at the NDBC buoy during the 283-day period, that is, 85% of the time, the H_s met or exceeded 0.5 m. When the H_s is 0.5 m, the coverage is only about 60% of its peak value, but the data quality is still good (Fig. 15).

6. Summary

Long-range CODAR SeaSonde HF radars and moored ADCP arrays have operated concurrently on the WFS since September 2003. We presented a performance evaluation for the period from September 2003 to May 2008 to assess the utility of such radars for mapping coastal ocean surface currents in a relatively low-energy (currents and waves) environment. Evaluations were made based on quantitative comparisons between HF radar-determined and in situ ADCP-measured currents. Along with rms differences these evaluations also included data return frequencies, bearing offsets, and radial velocity uncertainties for each of the radars. Such evaluations of 5-MHz, long-range, HF radar current estimates against long time series from several moored ADCPs adds a new contribution to the evolving HF radar community because most previous evaluations of HF radar currents were for higher frequency (12–25 MHz) radars deployed in more energetic (currents and waves) ocean environments and with fewer and shorter-duration in situ measurement sites for comparison.

Previous evaluations using a variety of data, including moored current meters, ship-mounted and moored ADCPs, and surface drifters (e.g., Teague 1986; Paduan and Rosenfeld 1996; Chapman et al. 1997; Graber et al. 1997; Kohut et al. 2006; Ohlmann et al. 2007; to name a few) yielded rmsd values of ~(5–20) cm s^{-1}. Despite the low-energy WFS environment and several other

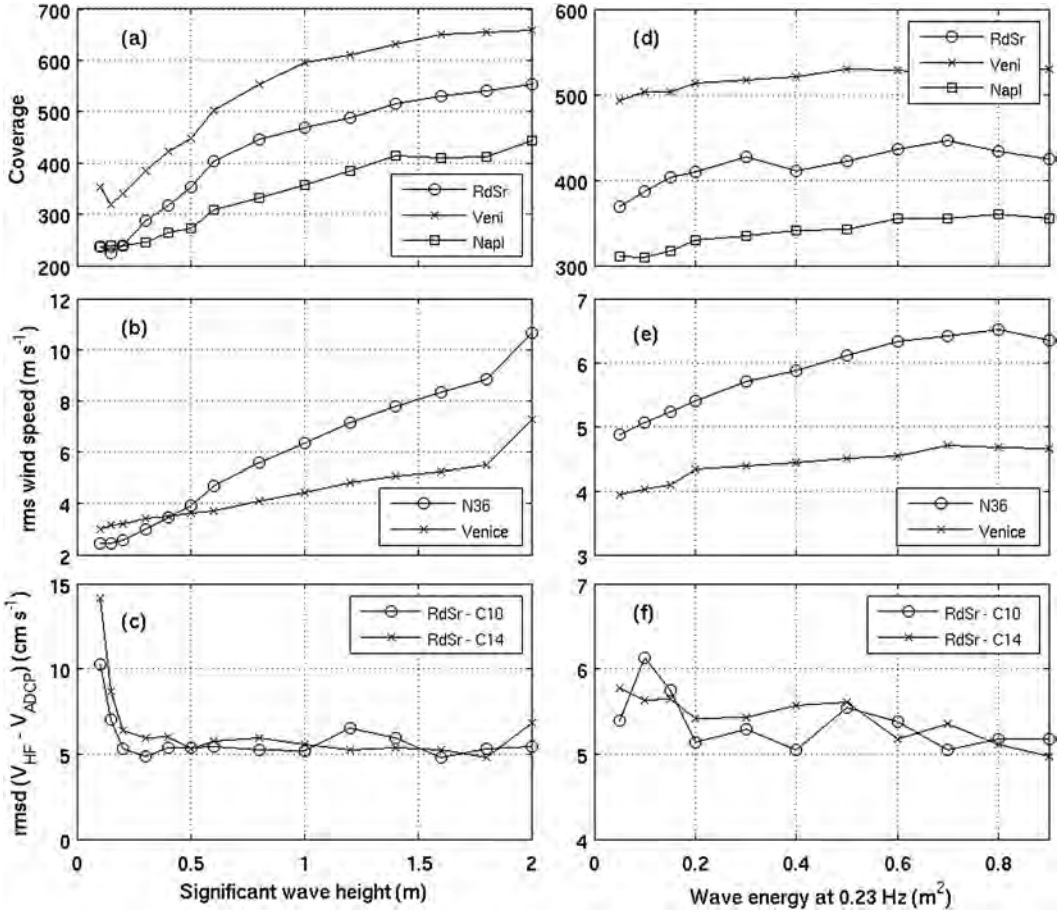

FIG. 15. Conditional averages of coverage (a), rms wind (b), rms current (c), and data quality as indicated by the rmsd of V_{HF} and V_{ADCP}; all binned by the H_s measured at NDBC buoy 42036. (d)–(f) as in (a)–(c), except that the averages are binned by the wave energy at 0.23 Hz measured at the same buoy.

challenges in achieving more continuous data returns, when acquired the data quality was found to be quite good. The rmsd values were in the range of 6–10 cm s^{-1} for hourly and 3–6 cm s^{-1} for 36-h low-pass-filtered radial currents, respectively. These rmsd values of HF radar–ADCP radial velocities are smaller than, or comparable to, those observed in many previous studies. Using winter months when higher-quality data were available, power spectra of the HF radar and ADCP radial currents compared favorably over both tidal and subtidal frequency bands, and good agreement was obtained for the major tidal constituents estimated from both data sources. The bearing offsets (uncertainties in radial velocity component placements) were found to be in the range from −15° to +9°, which were also similar to or slightly smaller than, those found in other studies (e.g., Emery et al. 2004; Paduan et al. 2006).

Notwithstanding satisfactory performance when data were available, the frequent data gaps (both temporally and spatially) were found to be problematic. On both synoptic and seasonal time scales, the temporal variations of the HF radar radial velocity component returns were found to be influenced by local wind and wave conditions. Generally, the radial coverage was best in winter and worst in summer, consistent with the seasonal fluctuations in wind speed, significant wave height, and the coastal ocean current speed. In essence, a combination of low backscatter resulting from small (or nonexistent) waves and weak currents, both modulated by wind, led to HF radar SNR falling below an effective HF radar noise level associated with the receiving antenna geometry and the manufacturer's signal-processing algorithm. Whereas this paper did not assess these technical factors explicitly, the findings were shown to be consistent with analyses from available directional surface wave energy information both observed and modeled.

As the winds and waves decreased ($H_s < 2$ m), so did the radial coverage, and the coverage decreased rapidly once the significant wave height dropped below 1 m. When the significant wave height decreased to 0.5 m,

the coverage decreased to about 60% of its peak value. However, the HF radar data quality (as measured by the rmsd between V_{HF} and V_{ADCP}) remained satisfactory until the significant wave height decreased below 0.3 m (corresponding to an rms wind speed of <3 m s^{-1} at the NDBC buoy location used).

In conclusion, the CODAR SeaSonde HF radar operation on the WFS shows that, when operable, the data are of similar quality as found elsewhere (when gauged quantitatively against in situ measurements by moored ADCPs). However, by virtue of the WFS low-energy environment it is apparent that a 5-MHz system suffers from data outages, especially in summer when winds (and hence waves) are small, causing SNR below an apparent performance threshold. Using a higher operational frequency may yield improvement [e.g., Shay et al. (2007) with a 12-MHz WERA system], but at the expense of range. The near future will see experimentation with a nominal 12-MHz WERA. Together the goal is to achieve both long- and shorter-range coverage as part of a comprehensive coastal ocean-observing system for the WFS.

Acknowledgments. Support was by the Office of Naval Research, Grants N00014-05-1-0483 and N00014-02-1-0972 and by NOAA Grant NA07NOS4730219-5032. The second of these, for the Southeast Atlantic Coastal Ocean Observing System (SEACOOS), was administered by UNC under Task Order 3-12110-10. The third is for the Southeast Coastal Ocean Observing Regional Association (SECOORA) administered by SC Sea Grant. The HF radar-processing toolbox HFR_Progs was provided by D. Kaplan, M. Cook, D. Atwater, and J. F. González. The Venice site was jointly maintained by Mote Marine Laboratory (B. Pederson and G. Kirkpatrick) and USF (C. Merz), with Rutgers University (H. Roarty and S. Glenn) providing the site equipment. The success of the seagoing activity at USF is attributed to R. Cole and J. Law, and J. Donovan, V. Subramanian, and D. Mayer assisted with real-time ADCP data acquisition and editing. Helpful discussions with CODAR staff (C. Whelan and H. Aguilar) are appreciated. Comments from four anonymous reviewers significantly improved the quality of the manuscript.

REFERENCES

Abascal, A. J., S. Castanedo, R. Medina, I. J. Losada, and E. Alvarez-Fanjul, 2009: Application of HF radar currents to oil spill modeling. *Mar. Pollut. Bull.,* **58,** 238–248.

Barrick, D. E., and B. J. Lipa, 1986: Correcting for distorted antenna patterns in CODAR ocean surface measurements. *IEEE J. Oceanic Eng.,* **OE-11,** 304–309.

——, and ——, 1997: Evolution of bearing determination in HF current mapping radars. *Oceanography,* **10,** 72–75.

——, M. W. Evans, and B. L. Weber, 1977: Ocean surface currents mapped by radar. *Science,* **198,** 138–144.

Barth, A., A. Alvera-Azcárate, and R. H. Weisberg, 2008: Assimilation of high-frequency radar currents in a nested model of the West Florida Shelf. *J. Geophys. Res.,* **113,** C08033, doi:10.1029/2007JC004585.

Beckenbach, E., and L. Washburn, 2004: Low-frequency waves in the Santa Barbara Channel observed by high-frequency radar. *J. Geophys. Res.,* **109,** C02010, doi:10.1029/2003JC001999.

Blaha, J., and W. Sturges, 1981: Evidence for wind-forced circulation in the Gulf of Mexico. *J. Mar. Res.,* **39,** 771–833.

Chant, R. J., S. Glenn, and J. Kohut, 2004: Flow reversals during upwelling conditions on the New Jersey inner shelf. *J. Geophys. Res.,* **109,** C12S03, doi:10.1029/2003JC001941.

Chapman, R. D., L. K. Shay, H. C. Graber, J. B. Edson, A. Karachintsev, C. L. Trump, and D. B. Ross, 1997: On the accuracy of HF radar surface current measurements: Intercomparisons with ship-based sensors. *J. Geophys. Res.,* **102** (C8), 18 737–18 748.

Chu, P. C., and K. F. Cheng, 2008: South China Sea wave characteristics during Typhoon Muifa passage in winter 2004. *J. Oceanogr.,* **64,** 1–21.

——, Y. Qi, Y. Chen, P. Shi, and Q. Mao, 2004: South China Sea wave characteristics. Part I: Validation of Wavewatch-III using TOPEX/Poseidon data. *J. Atmos. Oceanic Technol.,* **21,** 1718–1733.

Cook, T. M., T. de Paolo, and E. J. Terrill, 2007: Estimates of radial current error from high frequency radar using MUSIC for bearing determination. *Oceans 2007,* Vancouver, BC, Canada, IEEE, 1–6, doi:10.1109/OCEANS.2007.4449257.

Cosoli, S., M. Gacic, and A. Mazzoldi, 2005: Comparison between HF radar current data and moored ADCP current meter. *Nuovo Cimento,* **28C,** 6, 865–879, doi:10.1393/ncc/i2005-10032-6.

Crombie, D. D., 1955: Doppler spectrum of sea echo at 13.56Mc/s. *Nature,* **175,** 681–682.

Davies, K., 1990: *Ionospheric Radio*. IEEE Electromagnetic Waves Series, Vol. 31, Peter Peregrinus, 612 pp.

de Paolo, T., and E. J. Terrill, 2007: Skill assessment of resolving ocean surface current structure using compact-antenna-style HF radar and the MUSIC direction-finding algorithm. *J. Atmos. Oceanic Technol.,* **24,** 1277–1300.

Dzwonkowski, B., J. T. Kohut, and X.-H. Yan, 2009: Seasonal differences in wind-driven across-shelf forcing and response relationships in the shelf surface layer of the central Mid-Atlantic Bight. *J. Geophys. Res.,* **114,** C08018, doi:10.1029/2008JC004888.

Earle, M. D., K. E. Steele, and D. W. C. Wang, 1999: Use of advanced directional wave spectra analysis methods. *Ocean Eng.,* **26,** 1421–1434.

Ebuchi, N., Y. Fukamachi, K. I. Ohshima, K. Shirasawa, M. Ishikawa, T. Takatsuka, T. Daibo, and M. Wakatsuchi, 2006: Observation of the Soya Warm Current using HF ocean radar. *J. Oceanogr.,* **62,** 47–61, doi:10.1007/s10872-006-0031-0.

Emery, B. M., L. Washburn, and J. A. Harlan, 2004: Evaluating radial current measurements from CODAR high-frequency radars with moored current meters. *J. Atmos. Oceanic Technol.,* **21,** 1259–1271.

Emery, W. J., and R. E. Thomson, 2001: *Data Analysis Methods in Physical Oceanography*. 2nd ed. Elsevier, 654 pp.

Fernandez, D. M., L. A. Meadows, J. F. Vesecky, C. C. Teague, J. D. Paduan, and P. Hansen, 2000: Surface current measurements by HF radar in freshwater lakes. *IEEE J. Oceanic Eng.,* **25,** 458–471.

Gacic, M., V. Kovacevic, S. Cosoli, A. Mazzoldi, J. D. Paduan, I. Mancero-Mosquera, and S. Yar, 2009: Surface current patterns in front of the Venice Lagoon. *Estuarine Coastal Shelf Sci.,* **82,** 485–494.

Graber, H. C., D. R. Thompson, and R. E. Carande, 1996: Ocean surface features and currents measured with SAR interferometry and HF radar. *J. Geophys. Res.,* **101,** 25 813–25 832.

——, B. K. Haus, R. D. Chapman, and L. K. Shay, 1997: HF radar comparisons with moored estimates of current speed and direction: Expected differences and implications. *J. Geophys. Res.,* **102** (C8), 18 749–18 766.

Gurgel, K.-W., G. Antonischki, H.-H. Essen, and T. Schlick, 1999: Wellen Radar (WERA), a new ground-wave-based HF radar for ocean remote sensing. *Coastal Eng.,* **37,** 219–234.

Halper, F. B., and W. W. Schroeder, 1990: The response of shelf waters to the passage of tropical cyclones—Observations from the Gulf of Mexico. *Cont. Shelf Res.,* **10,** 777–793.

Haus, B. K., J. D. Wang, J. Rivera, J. Martinez-Pedraja, and N. Smith, 2000: Remote radar measurement of Shelf Currents of Key Largo, Florida. *Estuarine Coastal Shelf Sci.,* **51,** 553–569.

He, R., and R. H. Weisberg, 2002: Tides on the west Florida Shelf. *J. Phys. Oceanogr.,* **32,** 3455–3473.

Hisaki, Y., and C. Imadu, 2009: The southward recirculation of the East China Sea Kuroshio west of the Okinawa Island. *J. Geophys. Res.,* **114,** C06013, doi:10.1029/2008JC004943.

Ichikawa, K., R. Tokeshi, M. Kashima, K. Sato, T. Matsuoka, S. Kojima, and S. Fujii, 2008: Kuroshio variations in the upstream region as seen by HF radar and satellite altimetry data. *Int. J. Remote Sens.,* **29,** 6417–6426.

Kaplan, D. M., J. Largier, and L. W. Botsford, 2005: HF radar observations of surface circulation off Bodega Bay (northern California, USA). *J. Geophys. Res.,* **110,** C10020, doi:10.1029/2005JC002959.

——, C. Halle, J. Paduan, and J. L. Largier, 2009: Surface currents during anomalous upwelling seasons off central California. *J. Geophys. Res.,* **114,** C12026, doi:10.1029/2009JC005382.

Kelly, F. J., and Coauthors, 2002: An HF-radar test deployment amidst an ADCP array on the West Florida shelf. *Proc. Oceans 2002 Conf.,* Biloxi, MS, IEEE/MTS, 692–698.

Kim, S. Y., E. J. Terrill, and B. D. Cornuelle, 2008: Mapping surface currents from HF radar radial velocity measurements using optimal interpolation. *J. Geophys. Res.,* **113,** C10023, doi:10.1029/2007JC004244.

——, B. D. Cornuelle, and E. J. Terrill, 2009: Anisotropic response of surface currents to the wind in a coastal region. *J. Phys. Oceanogr.,* **39,** 1512–1533.

Kohut, J. T., and S. M. Glenn, 2003: Calibration of HF radar surface current measurements using measured antenna beam patterns. *J. Atmos. Oceanic Technol.,* **20,** 1303–1316.

——, ——, and D. Barrick, 1999: SeaSonde is integral to coastal flow model development. *Hydro Int.,* **3,** 32–35.

——, H. J. Roarty, and S. M. Glenn, 2006: Characterizing observed environmental variability with HF Doppler radar surface current mappers and acoustic Doppler current profilers: Environmental variability in the coastal ocean. *IEEE J. Oceanic Eng.,* **31,** 876–884.

——, ——, S. Licthenwalner, S. Glenn, D. Barrick, B. Lipa, and A. Allen, 2008: The Mid-Atlantic Regional Coastal Ocean Observing System: Serving Coast Guard needs in the Mid-Atlantic Bight. *US/EU-Baltic International Symposium,* Charlston, SC, IEEE/OES, doi:10.1109/CCM.2008.4480859.

Komar, P. D., and J. C. Allan, 2008: Increasing hurricane-generated wave heights along the U.S. East Coast and their climate controls. *J. Coastal Res.,* **24,** 479–488.

Kosro, P. M., 2005: On the spatial structure of coastal circulation off Newport, Oregon, during spring and summer 2001 in a region of varying shelf width. *J. Geophys. Res.,* **110,** C10S06, doi:10.1029/2004JC002769.

——, J. A. Barth, and T. P. Strub, 1997: The coastal jet: Observations of surface currents over the Oregon continental shelf from HF radar. *Oceanography,* **10,** 53–57.

Kovacevic, V., M. Gacic, I. Mancero-Mosquera, A. Mazzoldi, and S. Marinetti, 2004: HF radar observations in the northern Adriatic: Surface current field in front of the Venetian Lagoon. *J. Mar. Syst.,* **51,** 95–122.

Laws, K. E., D. M. Fernandez, and J. D. Paduan, 2000: Simulation based evaluations of HF radar ocean current algorithms. *IEEE J. Oceanic Eng.,* **25,** 481–491.

——, J. D. Paduan, and J. F. Vesecky, 2010: Estimation and assessment of errors related to antenna pattern distortion in CODAR SeaSonde high-frequency radar ocean current measurements. *J. Atmos. Oceanic Technol.,* **27,** 1029–1043.

Lipa, B. J., 2003: Uncertainties in SeaSonde current velocities. *Proc. IEEE/OES Seventh Working Conf. on Current Measurement Technology,* San Diego, CA, IEEE/OES, 1–6.

——, and D. E. Barrick, 1983: Least-squares method for the extraction of surface currents from CODAR cross-loop data: Application at ARSLOE. *IEEE J. Oceanic Eng.,* **OE-8,** 226–253.

——, B. Nyden, D. S. Ullman, and E. Terrill, 2006: SeaSonde radial velocities: Derivation and internal consistency. *IEEE J. Oceanic Eng.,* **31,** 850–860.

Lipphardt, B. L., Jr., A. D. Kirwan Jr., C. E. Grosch, J. K. Lewis, and J. D. Paduan, 2000: Blending HF radar and model velocities in Monterey Bay through normal mode analysis. *J. Geophys. Res.,* **105** (C2), 3425–3450.

Liu, Y., and R. H. Weisberg, 2005a: Momentum balance diagnoses for the West Florida Shelf. *Cont. Shelf Res.,* **25,** 2054–2074.

——, and ——, 2005b: Patterns of ocean current variability on the West Florida Shelf using the self-organizing map. *J. Geophys. Res.,* **110,** C06003, doi:10.1029/2004JC002786.

——, and ——, 2007: Ocean currents and sea surface heights estimated across the West Florida Shelf. *J. Phys. Oceanogr.,* **37,** 1697–1713.

——, ——, and C. N. K. Mooers, 2006: Performance evaluation of the self-organizing map for feature extraction. *J. Geophys. Res.,* **111,** C05018, doi:10.1029/2005JC003117.

——, ——, and L. K. Shay, 2007: Current patterns on the West Florida Shelf from joint self-organizing map analyses of HF radar and ADCP data. *J. Atmos. Oceanic Technol.,* **24,** 702–712.

——, P. MacCready, B. M. Hickey, E. P. Dever, P. M. Kosro, and N. S. Banas, 2009: Evaluation of a coastal ocean circulation model for the Columbia River plume in summer 2004. *J. Geophys. Res.,* **114,** C00B04, doi:10.1029/2008JC004929.

Marmorino, G. O., 1983a: Small-scale variations of the wind-driven coastal sea level response in the West Florida Bight. *J. Phys. Oceanogr.,* **13,** 93–102.

——, 1983b: Variability of current, temperature, and bottom pressure across the West Florida continental shelf, winter, 1981–1982. *J. Geophys. Res.,* **88** (C7), 4439–4457.

——, L. K. Shay, B. K. Haus, R. A. Handler, H. C. Graber, and M. P. Horne, 1999: An EOF analysis of HF Doppler radar current measurements of the Chesapeake Bay buoyant outflow. *Cont. Shelf Res.,* **19,** 271–288.

Mayer, D. A., J. I. Virmani, and R. H. Weisberg, 2007: Velocity comparisons from upward and downward acoustic Doppler current profilers on the West Florida Shelf. *J. Atmos. Oceanic Technol.,* **24,** 1950–1960.

Menéndez, M., F. J. Méndez, I. J. Losada, and N. E. Graham, 2008: Variability of extreme wave heights in the northeast Pacific Ocean based on buoy measurements. *Geophys. Res. Lett.,* **35,** L22607, doi:10.1029/2008GL035394.

Meyers, S. D., E. M. Siegel, and R. H. Weisberg, 2001: Observations of currents on the west Florida shelf break. *Geophys. Res. Lett.,* **28,** 2037–2040.

Mitchum, G. T., and W. Sturges, 1982: Wind-driven currents on the west Florida shelf. *J. Phys. Oceanogr.,* **12,** 1310–1317.

Molcard, A., P. M. Poulain, P. Forget, A. Griffa, Y. Barbin, J. Gaggelli, J. C. De Maistre, and M. Rixen, 2009: Comparison between VHF radar observations and data from drifter clusters in the Gulf of La Spezia (Mediterranean Sea). *J. Mar. Syst.,* **78** (Suppl.), S79–S89, doi:10.1016/j.jmarsys.2009.01.012.

Niiler, P. P., 1976: Observations of low-frequency currents on the West Florida continental shelf. *Mem. Soc. Roy. Sci. Liege,* **6,** 331–358.

Nishimoto, M. M., and L. Washburn, 2002: Patterns of coastal eddy circulation and abundance of pelagic juvenile fish in the Santa Barbara Channel, California, USA. *Mar. Ecol. Prog. Ser.,* **241,** 183–199.

Ohlmann, J. C., and P. P. Niiler, 2005: Circulation over the continental shelf in the northern Gulf of Mexico. *Prog. Oceanography,* **64,** 45–81.

——, P. White, L. Washburn, E. Terrill, B. Emery, and M. Otero, 2007: Interpretation of coastal HF radar-derived surface currents with high-resolution drifter data. *J. Atmos. Oceanic Technol.,* **24,** 666–680.

Oke, P. R., and Coauthors, 2002: A modeling study of the three-dimensional continental shelf circulation off Oregon. Part I: Model–data comparisons. *J. Phys. Oceanogr.,* **32,** 1360–1382.

Paduan, J. D., and L. K. Rosenfeld, 1996: Remotely sensed surface currents in Monterey Bay from shore-based HF radar (Coastal Ocean Dynamics Application Radar). *J. Geophys. Res.,* **101** (C9), 20 669–20 686.

——, and M. S. Cook, 1997: Mapping surface currents in Monterey Bay with CODAR type HF radar. *Oceanography,* **10,** 49–52.

——, and H. C. Graber, 1997: Introduction to high-frequency radar: Reality and myth. *Oceanography,* **10,** 36–39.

——, K. C. Kim, M. S. Cook, and F. P. Chavez, 2006: Calibration and validation of direction-finding high frequency radar ocean surface current observations. *IEEE J. Oceanic Eng.,* **31,** 862–875, doi:10.1109/JOE.2006.886195.

Parks, A. B., L. K. Shay, W. E. Johns, J. Martinez-Pedraja, and K.-W. Gurgel, 2009: HF radar observations of small-scale surface current variability in the Straits of Florida. *J. Geophys. Res.,* **114,** C08002, doi:10.1029/2008JC005025.

Pawlowicz, R., B. Beardsley, and S. Lentz, 2002: Classical tidal harmonic analysis including error estimates in MATLAB using T-TIDE. *Comput. Geosci.,* **28,** 929–937.

Prandle, D., and D. K. Ryder, 1985: Measurements of surface currents in Liverpool Bay by high-frequency radar. *Nature,* **315,** 128–131.

Price, J. F., C. N. K. Mooers, and J. C. VanLeer, 1978: Observation and simulation of storm-induced mixed-layer deepening. *J. Phys. Oceanogr.,* **8,** 582–599.

Ramp, S. R., D. E. Barrick, T. Ito, and M. S. Cook, 2008: Variability of the Kuroshio Current south of Sagami Bay as observed using long-range coastal HF radars. *J. Geophys. Res.,* **113,** C06024, doi:10.1029/2007JC004132.

Richman, J. G., R. A. de Szoeke, and R. E. Davis, 1987: Measurements of near-surface shear in the ocean. *J. Geophys. Res.,* **92** (C3), 2851–2858.

Roarty, H., J. Kohut, and S. Glenn, 2008: The Mid-Atlantic Regional Coastal Ocean Observing System: Serving Coast Guard and fisheries needs in the Mid-Atlantic Bight. *Proc. IEEE/OES/CMTC Ninth Working Conf. on Current Measurement Technology,* Charlston, SC, IEEE/OES/CMTC, 151–155.

Roughan, M., E. J. Terrill, J. L. Largier, and M. P. Otero, 2005: Observations of divergence and upwelling around Point Loma, California. *J. Geophys. Res.,* **110,** C04011, doi:10.1029/2004JC002662.

Schmidt, R. O., 1986: Multiple emitter location and signal parameter estimation. *IEEE Trans. Antennas Propag.,* **AP-34,** 276–280.

Sentchev, A., P. Forget, and Y. Barbin, 2009: Residual and tidal circulation revealed by VHF radar surface current measurements in the southern Channel Isles region (English Channel). *Estuarine Coastal Shelf Sci.,* **82,** 180–192.

Shay, L. K., H. C. Graber, D. B. Ross, and R. D. Chapman, 1995: Mesoscale surface current structure detected by HF radar. *J. Atmos. Oceanic Technol.,* **12,** 881–900.

——, S. J. Lentz, H. C. Graber, and B. K. Haus, 1998: Current structure variations detected by HF radar and vector measuring current meters. *J. Atmos. Oceanic Technol.,* **15,** 237–256.

——, T. M. Cook, H. Peters, A. J. Mariano, P. E. An, A. Soloviev, R. Weisberg, and M. Luther, 2002: Very high frequency radar mapping of surface currents. *IEEE J. Oceanic Eng.,* **27,** 155–169.

——, J. Martinez, T. M. Cook, B. K. Haus, and R. H. Weisberg, 2007: High frequency surface current mapping using Wellen Radar. *J. Atmos. Oceanic Technol.,* **24,** 484–503.

——, D. Savidge, R. Styles, H. Seim, and R. H. Weisberg, 2008: High-frequency radar observing systems in SEACOOS. *Mar. Technol. Soc. J.,* **42,** 55–67.

Shen, C. Y., and T. E. Evans, 2001: Surface-to-subsurface velocity projection for shallow water currents. *J. Geophys. Res.,* **106** (C4), 6973–6984.

Steele, K. E., C. C. Teng, and D. W. C. Wang, 1992: Wave direction measurements using pitch-roll buoys. *Ocean Eng.,* **19,** 349–375.

Stewart, R. H., and J. W. Joy, 1974: HF radio measurements of surface currents. *Deep-Sea Res.,* **21,** 1039–1049.

Takahashi, D., X. Guo, A. Morimoto, and S. Kojima, 2009: Biweekly periodic variation of the Kuroshio axis northeast of Taiwan as revealed by ocean high-frequency radar. *Cont. Shelf Res.,* **29,** 1896–1907.

Takeoka, H., Y. Tanaka, Y. Ohno, Y. Hisaki, A. Nadai, and H. Kuroiwa, 1995: Observation of the Kyucho in the Bungo Channel by HF radar. *J. Oceanogr.,* **51,** 699–711.

Teague, C. C., 1986: Multifrequency HF radar observations of currents and current shears. *IEEE J. Oceanic Eng.,* **11,** 258–269.

——, J. F. Vesecky, and Z. R. Hallock, 2001: A comparison of multifrequency HF radar and ADCP measurements of near-surface currents during COPE-3. *IEEE J. Oceanic Eng.,* **26,** 399–405.

Tolbert, W. H., and G. G. Salsman, 1964: Surface circulation of the eastern Gulf of Mexico as determined by drift-bottled studies. *J. Geophys. Res.,* **69,** 223–230.

Tolman, H. L., 1991: A third-generation model for wind waves on slowly varying, unsteady and inhomogeneous depths and currents. *J. Phys. Oceanogr.,* **21,** 782–797.

Ullman, D. S., and D. L. Codiga, 2004: Seasonal variation of a coastal jet in the Long Island Sound outflow region based on

HF radar and Doppler current observations. *J. Geophys. Res.,* **109,** C07S06, doi:10.1029/2002JC001660.

——, J. O'Donnell, J. Kohut, T. Fake, and A. Allen, 2006: Trajectory prediction using HF radar surface currents: Monte Carlo simulations of prediction uncertainties. *J. Geophys. Res.,* **111,** C12005, doi:10.1029/2006JC003715.

Warner, J. C., W. R. Geyer, and J. A. Lerczak, 2005: Numerical modeling of an estuary: A comprehensive skill assessment. *J. Geophys. Res.,* **110,** C05001, doi:10.1029/2004JC002691.

Weatherly, G. L., and P. J. Martin, 1978: On the structure and dynamics of the oceanic bottom boundary layer. *J. Phys. Oceanogr.,* **8,** 557–570.

——, and D. Thistle, 1997: On the wintertime currents in the Florida Big Bend region. *Cont. Shelf Res.,* **17,** 1297–1319.

Weisberg, R. H., B. D. Black, and H. Yang, 1996: Seasonal modulation of the west Florida continental shelf circulation. *Geophys. Res. Lett.,* **23,** 2247–2250.

——, ——, and Z. Li, 2000: An upwelling case study on Florida's west coast. *J. Geophys. Res.,* **105,** 11 459–11 469.

——, Z. Li, and F. E. Muller-Karger, 2001: West Florida shelf response to local wind forcing: April 1998. *J. Geophys. Res.,* **106,** 31 239–31 262.

——, R. He, Y. Liu, and J. Virmani, 2005: West Florida shelf circulation on synoptic, seasonal, and inter-annual time scales. *Circulation in the Gulf of Mexico: Observations and Models, Geophys. Monogr.,* Vol. 161, Amer. Geophys. Union, 325–347.

——, Y. Liu, and D. A. Mayer, 2009: West Florida Shelf mean circulation observed with long-term moorings. *Geophys. Res. Lett.,* **36,** L19610, doi:10.1029/2009GL040028.

Wilkin, J. L., 2006: The summertime heat budget and circulation of southeast New England shelf waters. *J. Phys. Oceanogr.,* **36,** 1997–2011.

Willmott, C. J., 1981: On the validation of models. *Phys. Geogr.,* **2,** 184–194.

Yang, H., R. H. Weisberg, P. P. Niiler, W. Sturges, and W. Johnson, 1999: Lagrangian circulation and forbidden zone on the West Florida Shelf. *Cont. Shelf Res.,* **19,** 1221–1245.

Yang, S., H. Ke, X. Wu, J. Tian, and J. Hou, 2005: HF radar ocean current algorithm based on MUSIC and the validation experiments. *IEEE J. Oceanic Eng.,* **30** (3), 601–618.

Yoshikawa, Y., T. Matsuno, K. Marubayashi, and K. Fukudome, 2007: A surface velocity spiral observed with ADCP and HF radar in the Tsushima Strait. *J. Geophys. Res.,* **112,** C06022, doi:10.1029/2006JC003625.

Zhu, D., L. Li, Y. Li, and X. Guo, 2008: Seasonal variation of surface currents in the southwestern Taiwan Strait observed with HF radar. *Chin. Sci. Bull.,* **53,** 2385–2391.